Reprinted from

CMES

Computer Modeling in Engineering & Sciences

Founder and Editor-in-Chief:
Satya N. Atluri

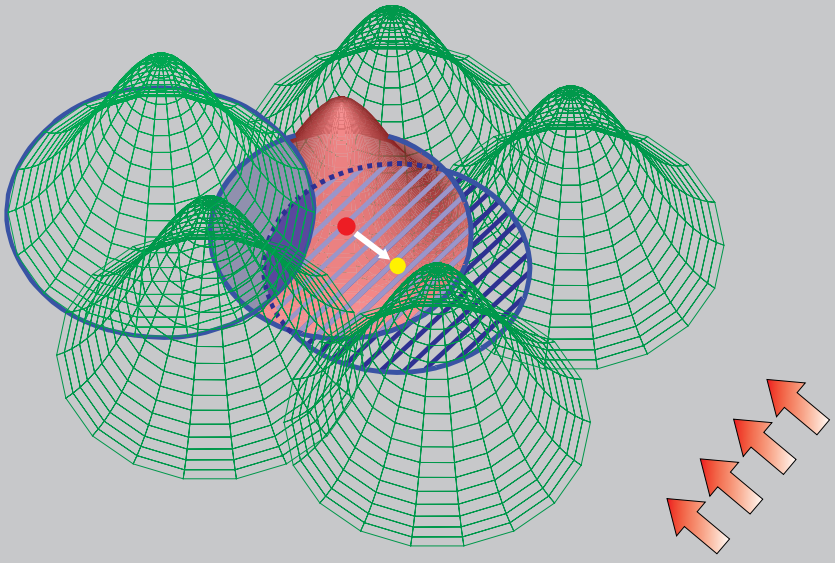

ISSN: 1526-1492 (print)
ISSN: 1526-1506 (on-line)

Tech Science Press

 CMES, vol.53, no.3, pp.255-302, 2009

A Unified Approach to Numerical Modeling of Fully and Partially Saturated Porous Materials by Considering Air Dissolved in Water

D. Gawin[1] **and L. Sanavia**[2]

Abstract: This paper presents a unified mathematical approach to model the hydro-thermo-mechanical behavior of saturated and partially saturated porous media by considering the effects of air dissolved in liquid water. The model equations are discretized by means of the Finite Element method. A correspondingly updated code is used to analyze two examples; the first one is the well known Liakopoulos test, i.e. the drainage of liquid water from a 1m column of sand, which is used to validate numerically the model here developed. As second example, a biaxial compression test of undrained dense sands where cavitation takes place at strain localization is simulated.
It is shown that considering the dissolved air has a small influence on the overall results of numerical simulations, while the histories of the fluid variables (gas and capillary pressure and water saturation) differ from other approaches neglecting the air dissolved. This may be important if appropriate constitutive models for partially saturated materials are used. A major advantage of the proposed procedure is that it allows for a unified modeling of partially and fully saturated zones in porous media without application of any 'unphysical' numerical technique.

Keywords: Poromechanics, Multiphase porous material, Coupled Thermo-Hydro-Mechanical modeling, Saturated-unsaturated transition, Air dissolution in liquid water, Water cavitation, Strain localization.

1 Introduction

In recent years, increasing interest in thermo-hydro-mechanical analysis of saturated and partially saturated porous materials is observed, because of a wide spectrum of their engineering applications. Typical examples belong to environmental

[1] Department of Building Physics and Building Materials, Technical University of Lodz, Al. Politechniki 6, 90-924 Lodz, Poland, e-mail: gawindar@p.lodz.pl
[2] Corresponding author. Dipartimento di Costruzioni e Trasporti, Universitá degli Studi di Padova, Via Marzolo 9, 35-131 Padova, Italy, e-mail: lorenzo.sanavia@unipd.it

geomechanics, where some challenging problems are of interest, e.g. the onset of landslides due to rainfall or earthquake, safety of deep nuclear waste disposal, land subsidence due to the extraction of water, oil or natural gas and that of sequestration of CO_2 in deep deposits.

In all the aforementioned situations, the soil needs to be considered as multiphase porous medium, made of a solid phase and closed and open pores containing one or more fluids, where the interaction between all the components of the material cannot be neglected.

The case with open pores is considered in this work, where the voids of the solid skeleton (made by solid grains) are filled with a liquid and a gas phase. The gas phase is assumed to be a mixture of dry air and water vapor, while the liquid phase is water, containing also dissolved air. (In the following the terms saturated and unsaturated are used in the traditional poro-mechanical sense. Hence, in a saturated porous medium the pores are fully filled with the liquid phase, while in partially saturated state the pores are partly filled with liquid and partly with one or more gaseous phases).

Most mathematical and numerical models for coupled Thermo-Hydro-Mechanical (THM) problems in porous media, also used in Geomechanics, [e.g. Zienkiewicz, Chan, Pastor, Paul, Shiomi (1990a); Zienkiewicz, Xie, Schrefler, Ladesma, Bicanic (1990b); Thomas, He, Sansom, Li (1994); Gawin and Schrefler (1996); Ehlers and Volk (1997); Lewis and Schrefler (1998); Zienkiewicz, Chan, Pastor, Schrefler, Shiomi (1999); de Boer (2000); Schrefler (2002); Coussy (2004), Borja (2004); Ehlers et al. (2004); Ferguson and Palananthakumar (2005), Sanavia, Pesavento and Schrefler (2006), Jabbari and Gatmiri (2007)], neglect the contribution of air dissolved in pore water. A general THM model considering air dissolved in pore water was theoretically formulated by Olivella, Carrera, Gens and Alonso (1994), Gens and Olivella (2001) and Khalili and Loret (2001). A numerical solution was presented in the work of Gens, Garcia-Molina, Olivella, Alonso and Huertas (1998), Gens and Olivella (2000) and Collin, Li, Radu and Charlier (2002), where the behavior of nuclear waste disposal was analyzed. In none of the above mentioned works the role of the effect of the dissolved air and its release on the gas phase on the numerical modeling has been analyzed in detail. A THM model considering the gas phase composed by water vapor and hydrogen and a liquid phase by water with dissolved hydrogen was developed by Gerard, Charlier, Barnichon, Su, Shao, Duveau, Giot, Chavant and Collin (2008).

Generally speaking, the dissolved air may play a role in the THM behavior of saturated/partially saturated porous media depending on its quantity and its variation in time. For example, 1 dm^3 of sand saturated with liquid water and having porosity of 20%, may contain at 20°C maximally about 3.98 ml of dissolved air at atmo-

spheric pressure (p_{atm}= 101325 Pa) and only 0.09 ml at pressure of 2339 Pa (i.e. at saturated vapor pressure value p^{gws} at 20 ˚C). The solubility of air in liquid water, according to Henry's law, Eq.1, decreases proportionally to the pressure drop, Eq.2, hence the excess amount of air is released in the form of small air bubbles. In general, this released air can contribute to the gas pressure in the zone, accelerating water desaturation and changing the pore pressure distribution. Moreover, it may play the role of nuclei for cavitation initiation, which can occur also in water saturated porous media, e.g. in case of compressive tests of undrained water saturated dense sand samples, Mokni and Desrues (1998); Vardoulakis and Sulem (1995); McManus and Davis (1997). Usually these experiments are performed by saturating the specimens with de-aired water and circulating fresh de-aired water in order to dissolve the rest of gas bubbles possibly trapped in the specimens and the circuits, Mokni and Desrues (1998). In field conditions this is not the case and hence the air dissolved in liquid water may influence the onset and evolution of water cavitation during strain localization.

Cavitation in initially water saturated and undrained dense sands was analyzed numerically by Schrefler, Sanavia and Majorana (1996) and Gawin, Sanavia and Schrefler (1998), where the so-defined isothermal monospecies approach and the isothermal two phase flow model have been developed, neglecting the heat effects of phase change during rapid evaporation of liquid water. These effects were taken into account in the non-isothermal three-phase model developed in the work of Sanavia, Pesavento and Schrefler (2006), where it was assumed that water vapor was the only gas present at cavitation. Then, the same problem was solved in Gawin and Sanavia (2010) with a simplified model including air dissolved in liquid water, where the influence of air released on the onset of cavitation was described.

In this paper, we further extend the mathematical model of coupled heat and mass transport in fully and partially saturated soils, [Sanavia, Pesavento and Schrefler (2006)] taking into account the dissolved air transport neglected in the work of Gawin and Sanavia (2010). This modeling approach will allow to deal in a unified way both with fully and partially saturated media and the transition between the two states with a sound physical model, without any additional unphysical assumptions, like for example the existence of a 'residual gas saturation' or the application of a special numerical 'switching' procedure during fully-partial saturation transition, Gawin and Schrefler (1996). We follow the idea of Vaunat, Gens and Jommi (1997), originally introduced for isothermal porous media and neglecting the effects of water phase changes, the non-advective fluxes and the velocity of the solid. Moreover, this model was developed by making use of the net stress concept. Here we use the approach for non-isothermal deforming porous materials considering water phase change and effect of material deformation due to generalized effec-

tive stress, which allows us to analyze water cavitation during strain localization in soils.

The paper is organized as follows. Physics of air dissolution and of water cavitation in porous media is summarized in Section 2; then, the mathematical model for non-isothermal multiphase porous media including dissolution of air in liquid water is derived in Section 3 at macroscopic level. Small strains and quasi-static loading conditions are assumed.

In Section 4 different numerical techniques used for modeling the transition between fully and partially saturated state in porous materials are discussed.

Finally, two numerical examples are solved in Section 5 with the finite element model derived from the developed mathematical model. These examples aim to analyze the effect of the dissolved air released on evolution of the transport processes in fully saturated geomaterials during two different desaturation processes and to compare the results with those obtained with the simplified model of Gawin and Sanavia (2010) and other two approaches usually adopted to model the transition from fully to partially saturated state. The first example simulates the Liakopoulos experiment (water outflow, due to gravity, from the bottom of a 1-m sand column, Liakopoulos 1965). The second example deals with the initiation and progress of cavitation phenomenon during strain localization in undrained water saturated dense sands.

2 Dissolution of air and cavitation in fully and partially saturated porous media

In this section, physics of air dissolution and its contribution to water cavitation in porous media is summarized for the sake of completeness following Gawin and Sanavia (2010).

Air dissolution (or in general, gas dissolution) in liquid water at equilibrium conditions can be described by Henry's law, e.g. in the following form, Atkins and de Paula (2002),

$$p_i^g = K_{xi} \cdot x_i = K_{ci} \cdot c_i \tag{1}$$

where p_i^g means the partial pressure of the gas component i and x_i and c_i are the mol fraction and concentration of the gas i in liquid water at equilibrium. K_{xi} and $K_{ci} = K_{xi} \cdot M_w / (\rho^w \cdot M_i)$ are the empirical Henry's law constants, dependent on water pressure p^w and temperature T; these constants are related to the mol fraction of gas component i in liquid water, $x_i = n_i / n_w$, or its concentration, $c_i = m_i / V_w$, respectively. M_w and M_i are molar masses, while n_w and n_i quantities of liquid

water and dissolved gas, expressed in moles, m_i is the mass, ρ^w the liquid water density and V_w the water volume. $x_i = n_i/n_w = \frac{m_a}{M_a}/\frac{m_w}{M_w}$.

This law is valid not only for positive water pressures (i.e. for water saturated porous media), as usually known (see e.g. Atkins and de Paula (2002), where the values of Henry's law constant for different gases at various positive pressure and temperature can be found) but also for partially saturated porous media including (absolute) negative water pressures, Mercury, Azaroual, Zeyen and Tardy (2003). Taking into account the data concerning solubility of different components of air in liquid water at negative pressures given by Mercury, Azaroual, Zeyen and Tardy (2003), the following approximate relationship for the air Henry's constant, K_{xa} [Pa], can be proposed:

$$\begin{aligned} K_{xa} = &\left[A_{p3}\cdot(p^w)^3 + A_{p2}\cdot(p^w)^2 + A_{p1}\cdot p^w + A_{p0}\right](T-273.15) \\ &+ B_{p3}\cdot(p^w)^3 + B_{p2}\cdot(p^w)^2 + B_{p1}\cdot p^w + B_{p0}, \end{aligned} \tag{2}$$

with A_{p3}= $1.322\cdot10^{-17}$ Pa^{-2} K^{-1}, A_{p2}= $6.558\cdot10^{-9}$ Pa^{-1} K^{-1}, A_{p1}= 1.249 K^{-1}, A_{p0}= $0.0972\cdot10^{9}$ Pa K^{-1}, and B_{p3}= $3.967\cdot10^{-16}$ Pa^{-2}, B_{p2}= $2.232\cdot10^{-7}$ Pa^{-1}, B_{p1}= $0.4814\cdot10^{2}$, B_{p0}= $4.138\cdot10^{9}$ Pa and where p^w [Pa] is the water pressure and T [K] the thermodynamic temperature. This relation gives results in good agreement with experimental (for $p^w > 0$) and theoretically predicted (for $p^w < 0$) data by Mercury, Azaroual, Zeyen and Tardy (2003) in the range from -200 MPa to 50 MPa, as shown in Fig. 1.

Using 1 Henry's law (1) and Eq.2, the pressure dependence of solubility of air in liquid water at different temperature and pressure is presented in Fig. 2.

When pressure of liquid water, containing initially the equilibrium concentration of dissolved air, decreases, an excess amount of air is liberated in the form of air bubbles, as will be explained in the following. The gas pressure in these bubbles is put equal to the sum of the water pressure, p^w, and the pressure exerted by a curved gas–water interface due to the surface tension, $\Delta p^c = 2\sigma_{wa}/R_b$, where σ_{wa} is the water-air surface tension and R_b is radius of the bubble. The gas in the bubbles is composed of water vapor and dry air hence, following Dalton's law of partial pressures, the gas pressure, p^g, is equal to the sum of vapor pressure, p^{gw}, and dry air pressure, p^{ga}. Taking into account the equilibrium condition on the bubble interface, one obtains:

$$p^{ga} + p^{gw} = p^w + \frac{2\sigma_{wa}}{R_b} \tag{3}$$

Assuming air to be a perfect gas, one can write Clapeyron's equation in the follow-

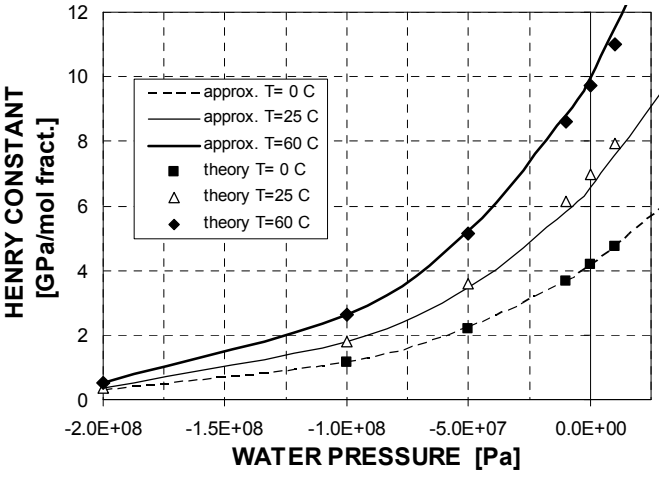

Figure 1: Comparison of the theoretical values of Henry's law constants for dry air, calculated from the data given by Mercury, Azaroual, Zeyen and Tardy (2003) and those obtained from approximation Eq.2 for different temperatures and pressures of water

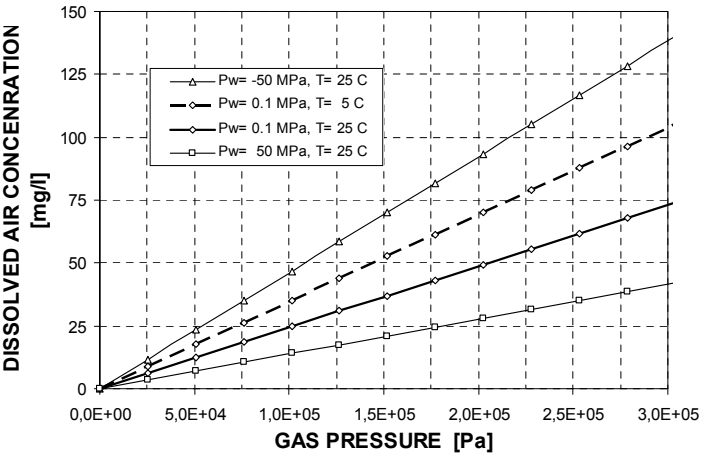

Figure 2: Dependence of the concentration of air dissolved in liquid water upon air pressure, for different values of pressure and temperature of liquid water

ing form:

$$p^{ga}V_{ga} = \frac{m_{ga}}{M_a}RT \tag{4}$$

where V_{ga} is the volume occupied by air, m_{ga} the dry air mass and R the universal gas constant. The air contained in the bubbles originates from that dissolved previously in liquid water due to pressure decrease, hence considering Henry's law, the mass of air released from the liquid water of volume V_w is:

$$m_{ga}^{rel} = \Delta c_{wa}V_w = \frac{p_0^{ga} - p^{ga}}{K_{ca}}V_w \tag{5}$$

with p_0^{ga} the dry air pressure initially dissolved in liquid water, Δc_{wa} the variation of the dissolved air concentration and K_{ca} the Henry law constant.

Assuming that air was initially dissolved in liquid water at atmospheric pressure, $p_0^{ga} = p_{atm}$, and taking into account Eq.3 and Eq.4, one obtains the following relationship describing the ratio of total volume of air, V_{ga}, released from the liquid water to its volume, V_w,

$$\frac{V_{ga}}{V_w} = \frac{RT}{M_a K_{ca}}\left(\frac{p_{atm}}{p^w + \frac{2\sigma_{wa}}{R_b} - p^{gw}} - 1\right) \tag{6}$$

Inside the air bubbles with radius greater than 10^{-6} m (capillary pressure $p^c < 1.46\ 10^5$ Pa), the relative humidity of air at temperature $T = 293.15$ K, according to the Kelvin equation (see e.g. Atkins and de Paula, 2002), exceeds 99 %RH, thus $p^{gw} \cong p^{gws} = 2338$ Pa.

The ratio V_{ga}/V_w can be interpreted as an additional degree of pore saturation with gas phase, $\Delta S_g = -\Delta S_w$. Fig. 3 shows dependence of the decrease of water saturation, $-\Delta S_w$, due to the release of air from water, upon the air bubble radius calculated from Eq.6. As can be observed from this figure, the greater is the bubble radius, the greater is the desaturation caused by the air released from liquid water. The radius increase is however constrained by the dimensions of pores, so one cannot expect that it will exceed a typical dimension of porosity. For example, for dense sands the latter is of order 10^{-5} m, thus one can expect that after decrease of water pressure to the value of $p^w = 2338$ Pa and creation of air bubbles with radius $R_b = 10^{-5}$ m, the air released from liquid water will cause desaturation $-\Delta S_w \cong 0.122$. For every water pressure, there exists a minimal value of air bubble radius, below which the surface tension, Δp^c, prevents creation of air bubbles due to the release of air dissolved in liquid water, because the latter is possible only if $p_{atm} > p^w + \frac{2\sigma_{wa}}{R_b} - p^{gw}$.

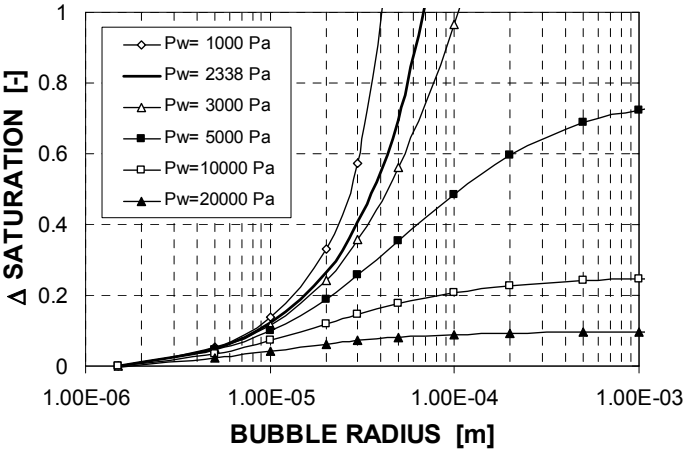

Figure 3: Dependence of the decrease of water saturation due to the release of air from liquid water upon the air bubble calculated from Eq.6

In addition to the acceleration of water desaturation, the excess amount of air released after water pressure decrease also may play a role of nuclei for cavitation initiation, as explained in what follows.

From the Classical Nucleation Theory, it is concluded that cavitation at low stretching pressures cannot practically be initiated by thermal fluctuations. In such conditions, the most important factor which could trigger cavitation nucleation in soils is the presence of impurities or (dissolved) air bubbles in liquid water, Or and Tuller (2002); Maris and Balibar (2000); Tyree (1997), because only bubbles with radius greater than a critical value, R_c, can grow freely (i.e. without energy supply) and can seed cavitation. The expression for the critical radius of air bubbles in liquid water, R_c, as a function of the capillary pressure, p^c, has been computed in Gawin and Sanavia (2010). The data presented there indicate that in capillary water both temperature and water pressure have a small influence upon the critical radius.

Fig. 4 shows the dependence of critical radius upon the water pressure under assumption that inside the bubble there is only vapor present, and not air. As can be observed, the critical radius has rather high values, exceeding typical pore radii of soils. So one cannot expect vapor bubbles will freely grow after cavitation onset.

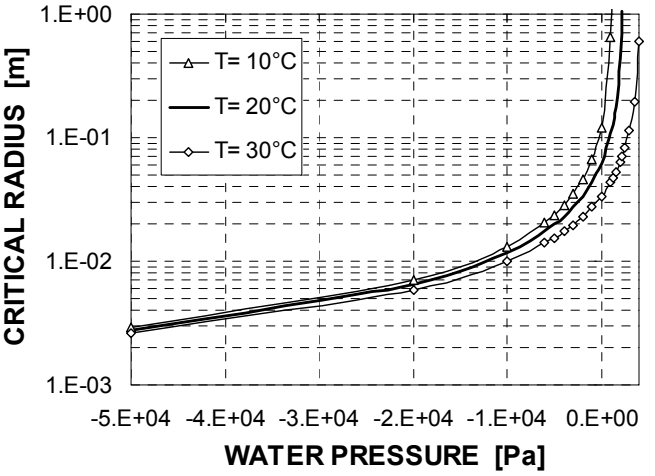

Figure 4: Dependence of the critical radius of vapor bubble at different water pressures and temperature

3 Macroscopic balance equations

The full mathematical model necessary to simulate the thermo-hydro-mechanical behavior of fully and partially saturated porous media, neglecting air dissolved in liquid water, was developed within the Hybrid Mixture Theory by Lewis and Schrefler (1998), Gawin and Schrefler (1996) and Schrefler (2002) using averaging theories according to Hassanizadeh and Gray (1979a), Hassanizadeh and Gray (1979b), Hassanizadeh and Gray (1980), Gray and Hassanizadeh (1991). The model which includes the air dissolved in pore water and the air mass source during its desorption at lower pressures will be now developed by taking into account the dissolved air transport phenomena neglected in the work of Gawin and Sanavia (2010). In comparison with the model neglecting air dissolved in liquid water, the new model is derived by suitable modification of the dry air mass balance equation, in which a source term will be introduced in the right hand side (Eq.11) given by a new equation, the dissolved air mass balance equation (12).

The partially saturated porous medium is treated as multiphase system composed of the solid skeleton (s) and voids filled with liquid water (w) containing dissolved air (wa) and gas (g). These gases are assumed to behave as an ideal mixture of dry air (non-condensable gas, ga) and water vapor (condensable one, gw).

At the macroscopic level the porous material is modeled by a substitute continuum

of volume B with boundary ∂B that simultaneously fills the entire domain, instead of the real fluids and the solid which fill only a part of it. In this substitute continuum each constituent π has a reduced density which is obtained through the volume fraction $\eta^{\pi}(\mathbf{x},t) = dv^{\pi}(\mathbf{x},t)/dv(\mathbf{x},t)$, where dv is the volume of the average volume element (representative elementary volume, REV) of the porous medium and dv^{π} is the volume occupied by the constituent π in dv. $\mathbf{x}$ is the vector of the spatial coordinates and t the current time.

The solid is deformable and non-polar, and the fluids, solid and thermal fields are coupled. The constituents are assumed to be isotropic, homogeneous, immiscible except for dry air and vapor, and chemically non-reacting. At micro level, solid and water constituents are incompressible, while gas is considered compressible. Local thermal equilibrium between solid matrix, gas and liquid phases is assumed, so that the temperature is the same for all the constituents. In the developed model heat conduction and convection, vapor diffusion, water flow due to pressure gradients or capillary effects and water phase change (evaporation and condensation) inside the pores are taken into account.

In the partially saturated zones the liquid water is separated from its vapor by a meniscus concave toward gas (capillary water). Due to the curvature of this meniscus the sorption equilibrium equation (Gray and Hassanizadeh, 1991) gives the relationship $p^c = p^g - p^w$ between the capillary, gas and water pressure. Water pressure is defined as compressive positive, while stress in the solid is defined as tension positive.

The balance equations of the model are now derived at macroscopic level in the geometrically linear setting and for quasi-static loading conditions. The primary variables are chosen to be the displacements of the solid matrix, $\mathbf{u}(\mathbf{x},t)$, the capillary and gas pressure, $p^c(\mathbf{x},t)$ and $p^g(\mathbf{x},t)$, respectively, and the absolute temperature, $T(\mathbf{x},t)$. For a detailed discussion about the chosen fluids' primary variables see Sanavia, Pesavento and Schrefler (2006). Moreover, as usual in multiphase porous media theory, the motion of the solid is assumed as a reference, while that of the fluids is described with respect to the solid (which means that the fluid relative velocity $\mathbf{v}^{\pi s} = \mathbf{v}^{\pi} - \mathbf{v}^{s}$ is introduced, with $\pi = w$, *g, ga, gw, wa* and $\mathbf{v}^{s} = \frac{\partial \mathbf{u}}{\partial t}$ the velocity of the solid matrix).

The equilibrium equation of the mixture in terms of generalized effective stress $\boldsymbol{\sigma}'(\mathbf{x},t)$ assumes the form

$$div\left(\boldsymbol{\sigma}' - [p^g - S_w p^c]\,\mathbf{1}\right) + \rho\mathbf{g} = \mathbf{0} \tag{7}$$

where $\rho = [1-n]\,\rho^s + nS_w\rho^w + nS_g\rho^g$ is the mass density of the overall medium, $n(\mathbf{x},t)$= 1-η^s the porosity, $S_w(\mathbf{x},t)$ and $S_g(\mathbf{x},t)$ the water and gas degree of saturation, respectively (S_w + S_g =1; η^w=nS_w; η^g=nS_g). ρ^{π} is the microscopic or bulk

mass density ($\pi = s, w, g$), $\mathbf{g}$ the gravity acceleration vector and $\mathbf{1}$ the second order identity tensor.

The total stress of Eq.7, using saturation as weighting functions for capillary pressure was introduced by Schrefler (1984) using volume averaging for the bulk materials and is thermodynamically consistent, Gray and Hassanizadeh (1991), Gray and Schrefler (2001), Borja (2004).

The mass balance equations for the liquid water and its vapor are, respectively, Gawin and Schrefler (1996), Lewis and Schrefler (1998),

$$n\rho^w \frac{\partial S_w}{\partial t} + \rho^w S_w div\,\mathbf{v}^s - \beta_s \rho^w [1-n] S_w \frac{\partial T}{\partial t} + div\left(\rho^w \frac{\mathbf{k}k^{rw}}{\mu^w}[-grad\,(p^w) + \rho^w \mathbf{g}]\right) = -\dot{m}_{gw}, \quad (8)$$

and

$$-n\rho^{gw}\frac{\partial S_g}{\partial t} + \rho^{gw}[1-S_w]\,div\,\mathbf{v}^s + nS_g\frac{\partial \rho^{gw}}{\partial t} - \beta_s\rho^{gw}[1-n][1-S_w]\frac{\partial T}{\partial t}$$
$$-div\left(\rho^g \frac{M_a M_w}{M_g^2}\mathbf{D}_g^{gw} grad\left(\frac{p^{gw}}{p^g}\right)\right) + div\left(\rho^{gw}\frac{\mathbf{k}k^{rg}}{\mu^g}[-grad\,(p^g) + \rho^g\mathbf{g}]\right) = \dot{m}_{gw}, \quad (9)$$

where $\mathbf{k}(\mathbf{x},t)$=$k(\mathbf{x},t)\mathbf{1}$ is the intrinsic permeability tensor of the porous matrix in saturated condition [m^2], $k^{r\pi}(\mathbf{x},t)$ the fluid relative permeability parameter (a dimensionless parameter varying from zero to one) and $\mu^{\pi}(x, t)$ the dynamic viscosity of fluid [Pa·s], with $\pi = w, g$, while $\dot{m}_{gw}$ is the mass rate of water evaporation. $\beta_s(x, t)$ means the cubic thermal expansion coefficient of solid. $\mathbf{D}_g^{gw}(\mathbf{x})$ is the effective diffusivity tensor of water vapor (the diffusing phase) in the gas phase (the phase in which diffusion takes place) contained in the pore space, function of the tortuosity factor, and M_a, M_w and $M_g(\mathbf{x},t)$ the molar mass of dry air, liquid water and gas mixture, respectively. $M_g = \left[\frac{\rho^{gw}}{\rho^g}\frac{1}{M_w} + \frac{\rho^{ga}}{\rho^g}\frac{1}{M_a}\right]^{-1}$. These equations contain the mass balance equation of the solid phase, which has been introduced to eliminate the time derivative of the porosity, Gawin and Schrefler (1996), Lewis and Schrefler (1998).

The source term in Eq.8 is eliminated by summing it up with Eq.9, yielding the

water species mass balance equation

$$
\begin{aligned}
& n\left[\rho^{w}-\rho^{gw}\right]\frac{\partial S_{w}}{\partial t}+\left[\rho^{w}S_{w}+\rho^{gw}S_{g}\right]div\,\mathbf{v}^{s}+nS_{g}\frac{\partial\rho^{gw}}{\partial t} \\
& -div\left(\rho^{g}\frac{M_{a}M_{w}}{M_{g}^{2}}\mathbf{D}_{g}^{gw}grad\left(\frac{p^{gw}}{p^{g}}\right)\right)-div\left(\rho^{gw}\frac{\mathbf{k}k^{rg}}{\mu^{g}}\left[grad\left(p^{g}\right)-\rho^{g}\mathbf{g}\right]\right) \\
& +div\left(\rho^{w}\frac{\mathbf{k}k^{rw}}{\mu^{w}}\left[-grad\left(p^{g}-p^{c}\right)+\rho^{w}\mathbf{g}\right]\right)-\beta_{sgw}\frac{\partial T}{\partial t}=0
\end{aligned}
\tag{10}
$$

where $\beta_{swg}=[1-n]\beta_{s}[S_{g}\rho^{gw}+\rho^{w}S_{w}]$.

In Eq.8-10 the advective fluxes have been described by using Darcy's law for liquid water and gas, while the diffusion of vapor in the gas phase has been modeled with Fick's law.

The mass balance equation for the dry air is:

$$
\begin{aligned}
& -n\rho^{ga}\frac{\partial S_{w}}{\partial t}+\rho^{ga}\left[1-S_{w}\right]div\,\mathbf{v}^{s}+n\left[1-S_{w}\right]\frac{\partial\rho^{ga}}{\partial t} \\
& -div\left(\rho^{g}\frac{M_{a}M_{w}}{M_{g}^{2}}\mathbf{D}_{g}^{ga}grad\left(\frac{p^{ga}}{p^{g}}\right)\right)+div\left(\rho^{ga}\frac{\mathbf{k}k^{rg}}{\mu^{g}}\left[-grad\left(p^{g}\right)+\rho^{g}\mathbf{g}\right]\right) \\
& -\left[1-n\right]\beta_{s}\left[1-S_{w}\right]\rho^{ga}\frac{\partial T}{\partial t}=\dot{m}_{ga}.
\end{aligned}
\tag{11}
$$

where $\mathbf{D}_{g}^{ga}(x,t)=D_{g}^{ga}\mathbf{1}$ is the effective diffusivity tensor of dry air in water vapor.

In Eq.11 $\dot{m}_{ga}$ is the new term (with respect to the model neglecting the air dissolved in water) which describes the rate of dry air mass released in the gas phase by desorption of the air dissolved in water. This quantity can be obtained from the mass balance of the dissolved air, which has the following form:

$$
\begin{aligned}
& nc_{wa}\frac{\partial S_{w}}{\partial t}+c_{wa}S_{w}div\,\mathbf{v}^{s}+nS_{w}\frac{\partial c_{wa}}{\partial t}-\left[1-n\right]\beta_{s}c_{wa}S_{w}\frac{\partial T}{\partial t}-div\left[\mathbf{D}_{w}^{ga}grad\left(c_{wa}\right)\right] \\
& +div\left(c_{wa}\frac{\mathbf{k}k^{rw}}{\mu^{w}}\left[-grad\left(p^{g}-p^{c}\right)+\rho^{w}\mathbf{g}\right]\right)=-\dot{m}_{ga},
\end{aligned}
\tag{12}
$$

where $c_{wa}(\mathbf{x},t)$ is the concentration of air dissolved in water and $\mathbf{D}_{w}^{ga}(\mathbf{x})=D_{w}^{ga}\mathbf{1}$ the effective diffusivity tensor of the dissolved air in liquid water contained in the pore space.

In the development of the final model, the source RHS term in Eq.11 is eliminated by summing it up with Eq.12, resulting in the air species mass balance equation of

the following form,

$$
\begin{aligned}
&n\left[c_{wa}-\rho^{ga}\right]\frac{\partial S_w}{\partial t}+\left[c_{wa}S_w+\rho^{ga}S_g\right]div\,\mathbf{v}^s-\beta_{saw}\frac{\partial T}{\partial t}+n\left[1-S_w\right]\frac{\partial \rho^{ga}}{\partial t}+nS_w\frac{\partial c_{wa}}{\partial t}\\
&-div\left(\rho^g\frac{M_aM_w}{M_g^2}\mathbf{D}_g^{ga}grad\left(\frac{p^{ga}}{p^g}\right)\right)+div\left(\rho^{ga}\frac{\mathbf{k}k^{rg}}{\mu^g}\left[-grad\left(p^g\right)+\rho^g\mathbf{g}\right]\right)\\
&-div\left(\mathbf{D}_w^{ga}grad\left(c_{wa}\right)\right)+div\left(c_{wa}\frac{\mathbf{k}k^{rw}}{\mu^w}\left[-grad\left(p^g-p^c\right)+\rho^w\mathbf{g}\right]\right)=0
\end{aligned}
\tag{13}
$$

where $\beta_{saw}=\beta_s\left[1-n\right]\left[\rho^{ga}S_g+c_{wa}S_w\right]$.
Considering the Henry law, $c_{wa}=p^{ga}/K_{ca}$, Eq.13 can be expressed in terms of the common variable, p^{ga}, describing both the state of gaseous and dissolved air,

$$
\begin{aligned}
&n\left[\frac{p^{ga}}{K_{ca}}-\rho^{ga}\right]\frac{\partial S_w}{\partial t}+\left[\frac{p^{ga}}{K_{ca}}S_w+\rho^{ga}\left[1-S_w\right]\right]div\,\mathbf{v}^s\\
&+n\left[1-S_w\right]\frac{\partial \rho^{ga}}{\partial t}+nS_w\frac{\partial}{\partial t}\left(\frac{p^{ga}}{K_{ca}}\right)\\
&-div\left(\rho^g\frac{M_aM_w}{M_g^2}\mathbf{D}_g^{ga}grad\left(\frac{p^{ga}}{p^g}\right)\right)+div\left(\rho^{ga}\frac{\mathbf{k}k^{rg}}{\mu^g}\left[-grad\left(p^g\right)+\rho^g\mathbf{g}\right]\right)\\
&-div\left(\mathbf{D}_w^{ga}grad\left(\frac{p^{ga}}{K_{ca}}\right)\right)-\beta_{saw}\frac{\partial T}{\partial t}+div\left(\frac{p^{ga}}{K_{ca}}\frac{\mathbf{k}k^{rw}}{\mu^w}\left[-grad\left(p^g-p^c\right)+\rho^w\mathbf{g}\right]\right)\\
&=0.
\end{aligned}
\tag{14}
$$

One should underline that this equation makes physical sense both for partial and fully saturated porous media. In fact, when considering water flow in a fully saturated porous material (S_w= 1), all the terms in Eq.14 related to gaseous phase are equal to zero and can be omitted and the air species mass balance Eq.14 is reduced to

$$
\begin{aligned}
&\frac{p^{ga}}{K_{ca}}div\,\mathbf{v}^s+n\frac{\partial}{\partial t}\left(\frac{p^{ga}}{K_{ca}}\right)-\beta_{saw}\frac{\partial T}{\partial t}-div\left(\mathbf{D}_w^{ga}grad\frac{p^{ga}}{K_{ca}}\right)\\
&+div\left(\frac{p^{ga}}{K_{ca}}\frac{\mathbf{k}k^{rw}}{\mu^w}\left[grad\left(p^c\right)+\rho^w\mathbf{g}\right]\right)=0
\end{aligned}
\tag{15}
$$

where the pressure p^c is in the range of negative values ($p^c \leq 0$) and means the excess water pressure relative to the atmospheric pressure p_{atm}, as explained in

Section 4 and by Gawin and Schrefler (1996). Atmospheric pressure is usually assumed to be constant, from which follows the relationship $grad\,(p^w) = -grad\,(p^c)$ introduced in the last term of Eq.15.

For fully saturated materials, the pressure p^{ga} in Eq.15 means a value of dry air pressure being in thermodynamic equilibrium with the air dissolved actually in the liquid water. This variable is preferred here for the description of the concentration of air dissolved in water to avoid introducing directly into the mathematical model an additional state variable, c_{wa}. This is possible because at full saturation no gaseous phase is present in the pores and the variables p^g and p^{ga} are not used. Thus, such a choice assures continuity of the variable both at the interface between the full and partial saturated state of a porous medium and during the transition between these states.

Moreover, the formulation obtained so far has also advantages from the numerical point of view because it allows to avoid application of a residual saturation (which means the presence of gas in the "fully water saturated" material), or of an appropriate switching procedure to eliminate the gas mass conservation equation for fully saturated material, see Gawin and Schrefler (1996). Also, it allows for efficient modeling 'full - partial saturation' transition without formulating the related Stefan problem, as will be explained in Section 4.

The model for fully saturated materials is completed by the liquid water mass balance equation of the following form

$$\rho^w div\,\mathbf{v}^s - \beta_{sw}\frac{\partial T}{\partial t} + div\left(\rho^w \frac{\mathbf{k}k^{rw}}{\mu^w}\left[grad\,(p^c) + \rho^w \mathbf{g}\right]\right) = 0 \tag{16}$$

which is a reduced form of Eq.10, where β_{sw} =[1-n]$\beta_s\rho^w$. Then, we need the enthalpy balance equation

$$(\rho C_p)_{eff}\frac{\partial T}{\partial t} + n\rho^w C_p^w \mathbf{v}^{ws}\cdot grad\,T - div\,(\chi_{eff} grad\,T) = 0 \tag{17}$$

and the equilibrium equation

$$div\left(\sigma' - p^w\mathbf{1}\right) + \rho\mathbf{g} = \mathbf{0} \tag{18}$$

which are derived from Eq.19 and Eq.7, respectively. $\rho = [1-n]\,\rho^s + n\rho^w$.

For partially saturated materials the balance equations (7), (10) and (14) are completed by the enthalpy balance equation of the mixture written as Gawin and Schrefler (1996), Lewis and Schrefler (1998):

$$(\rho C_p)_{eff}\frac{\partial T}{\partial t} + \left[nS_w\rho^w C_p^w \mathbf{v}^{ws} + nS_g\rho^g C_p^g \mathbf{v}^{gs}\right]\cdot grad\,T - div\,(\chi_{eff} grad\,T) = -\dot{m}_{gw}\Delta H_{vap} \tag{19}$$

where $(\rho C_p)_{eff}(x, t)$ is the effective thermal capacity of the porous medium, $C_p^w(x, t)$ and $C_p^g(x, t)$ the specific heat of water and gas mixture, respectively. $\chi_{eff}(x, t)$ the effective thermal conductivity of the porous medium and ΔH_{vap} the latent heat of evaporation. $\dot{m}_{gw}$ is given by the balance equation for liquid water, Eq.8. The right hand side term of Eq.19 considers the contribution of evaporation and condensation. This balance equation takes into account the heat transfer through conduction and convection as well as latent heat transfer and neglects the terms related to the mechanical work induced by density variations due to temperature changes of the phases and induced by volume fraction changes (a more general balance equation is developed by Khalili and Loret, 2001).

3.1 Simplified form of the air mass balance equation

The dissolved air mass balance equation (14) for partially saturated state can be simplified by omitting the terms with values which are small in comparison to the other ones.

Considering the Clapeyron equation for the dry air, $\rho^{ga} = p^{ga} M_a / RT$, one can assume that:
$\frac{p^{ga}}{K_{ca}} - \rho^{ga} = \left[\frac{1}{K_{ca}} - \frac{M_a}{RT}\right] p^{ga} \approx -\frac{M_a}{RT} p^{ga} = -\rho^{ga}$, because at T=298.15 K the first term in the parenthesis, $\frac{1}{K_{ca}} = \frac{1}{6.6 \cdot 10^9} \approx 1.5 \cdot 10^{-10} \left[\frac{\text{kg}}{\text{J}}\right]$, is small in comparison to the second one, $\frac{M_a}{RT} = \frac{0.02884}{2479} \approx 1.15 \cdot 10^{-5} \left[\frac{\text{kg}}{\text{J}}\right]$. Then, the term related to advective transport of dissolved air, caused by the gas gradient, is equal to $\frac{1}{K_{ca}} \frac{p^{ga}}{\mu_w} \approx \frac{1.15 \cdot 10^{-10}}{10^{-3}} p^{ga} = 1.15 \cdot 10^{-7} p^{ga} \left[\frac{\text{s}}{\text{m}^2}\right]$, while the term related to advective air flux $\frac{\rho^{ga}}{\mu^g} = \frac{M_a}{RT} \frac{1}{\mu_g} p^{ga} = \frac{1.15 \cdot 10^{-5}}{1.83 \cdot 10^{-5}} p^{ga} \approx 0.63 p^{ga} \left[\frac{\text{s}}{\text{m}^2}\right]$ is much larger, hence the dissolved air flux due to the gradient of gas pressure can be omitted in comparison to the advective air mass flux.

Moreover, in many cases occurring in practice, e.g. in soil mechanics, the gas pressure within the pores of partially saturated material is usually very close to the (constant) atmospheric pressure, $p^g \approx p_{atm}$, thus $grad\left(\frac{p^{ga}}{p^g}\right) \approx \frac{grad(p^{ga})}{p^g}$, and assuming that $M_a \approx M_g$, it follows that the term related to the diffusive flux of air molecules in the gas phase has the value of

$$\frac{\rho^g}{p^g} \frac{M_a M_w}{M_g^2} D_g^{ga} = \frac{M_g}{RT} \frac{M_a M_w}{M_g^2} D_g^{ga} \approx \frac{M_w}{RT} D_g^{ga} = \frac{0.018}{2479} 0.24 \cdot 10^{-4} \approx 1.74 \cdot 10^{-10} \,[\text{s}]$$

Then, in normal situations the Henry law parameter has practically the same value,

K_{ca}= const, hence $grad\left(\frac{p^{ga}}{K_{ca}}\right) \approx \frac{grad(p^{ga})}{K_{ca}}$ and the term for the diffusive flux of air dissolved in liquid water is $\frac{1}{K_{ca}} D_w^{ga} = 1.5 \cdot 10^{-10} \cdot 1.97 \cdot 10^{-5} = 2.96 \cdot 10^{-15}$ [s]; it follows that the air diffusive flux in liquid water can be neglected in comparison to the flux in gas phase.

Finally, with the aforementioned simplifications, the mass balance equation of dry air for partially saturated medium is of the following form:

$$\begin{aligned} &-n\rho^{ga}\frac{\partial S_w}{\partial t} + \left[\frac{p^{ga}}{K_{ca}} S_w + \rho^{ga}\left[1-S_w\right]\right] div\,\mathbf{v}^s - \beta_{saw}\frac{\partial T}{\partial t} \\ &+ n\left[1-S_w\right]\frac{\partial \rho^{ga}}{\partial t} + nS_w\frac{\partial}{\partial t}\left(\frac{p^{ga}}{K_{ca}}\right) \\ &- div\left(\rho^g \frac{M_a M_w}{M_g^2}\mathbf{D}_g^{ga} grad\left(\frac{p^{ga}}{p^g}\right)\right) + div\left(\rho^{ga}\frac{\mathbf{k}k^{rg}}{\mu^g}\left[-grad\left(p^g\right) + \rho^g\mathbf{g}\right]\right) \\ &+ div\left(\frac{p^{ga}}{K_{ca}}\rho^w\frac{\mathbf{k}k^{rw}}{\mu^w}\left[grad\left(p^c\right) + \rho^w\mathbf{g}\right]\right) = 0. \end{aligned} \tag{20}$$

In comparison to the air mass balance equation not considering the dissolved air effects, Eq.11, one can observe three main additional terms. The first one is related to the changes of dissolved air content due to volumetric strains of material, the second one defines the mass source/sink of air due to desorption/dissolution of air in liquid water, and the last one describes the advective transport of the air dissolved in liquid water. It is worth to underline that Eq.20 automatically transforms into the Eq.15, valid for the fully saturated medium (S_w= 1), if one accounts that all the terms containing (1-S_w) and $\frac{\partial S_w}{\partial t}$ are equal to zero. Then, it takes additionally into consideration the diffusive flux of air dissolved in liquid water, which is negligible in the partially saturated state. The diffusive flux can be also omitted for the fully saturated medium when there are considerable gradients of water pressure or when one analyzes relatively fast phenomena, i.e. with the characteristic time visibly smaller than that for the diffusion of air in water, $\tau_c = d^2/D_w^{ga}$ (d is characteristic dimension of an analyzed element), e.g. for d= 0.1 m one obtains the characteristic time $\tau_c \approx \left(10^{-1}\right)^2/1.97 \cdot 10^{-5} \approx 500\,[s]$.

3.2 Constitutive equations

For a gaseous mixture of dry air and water vapor, the ideal gas law is introduced because the moist air is assumed to be a perfect mixture of two ideal gases. The equation of state of perfect gas (Clapeyron's equation) and Dalton's law applied to dry air (ga), water vapor (gw) and moist air (g), yields

$$p^{ga} = \rho^{ga} TR/M_a, \quad p^{gw} = \rho^{gw} TR/M_w, \quad p^g = p^{ga} + p^{gw}, \quad \rho^g = \rho^{ga} + \rho^{gw} \tag{21}$$

In the partially saturated zones, the equilibrium water vapor pressure $p^{gw}(\mathbf{x},t)$ can be obtained from the Kelvin-Laplace equation, where the water vapor saturation pressure, p^{gws}, depending only upon the temperature, can be calculated from the Clausius-Clapeyron equation or from an empirical correlation. In fully saturated zones, for the sake of physical and mathematical consistency, it is assumed that the air pressure, despite of its different meaning, is related to the state variable p^g as follows, $p^{ga} = p^g - p^{gws}$, which corresponds to Dalton's law.

The saturation degree $S_\pi(\mathbf{x},t)$ and the relative permeability $k^{r\pi}(\mathbf{x},t)$ are experimentally determined functions of the capillary pressure and the temperature.

The solid skeleton is assumed elasto-plastic, homogeneous and isotropic; its mechanical behavior is described within the classical rate-independent elasto-plasticity theory for geometrically linear problems. For the second numerical example, the yield function restricting the effective stress state $\boldsymbol{\sigma}'(\mathbf{x},t)$ is developed in the form of temperature independent Drucker-Prager model for simplicity, with linear isotropic softening and non-associated plastic flow to take into account the post-peak and dilatant behavior of dense sands, respectively (see e.g. Selvadurai and Ghiabi, 2008). The return mapping and the consistent tangent operator for the Jacobian matrix, Eq.29, is developed by Sanavia, Pesavento and Schrefler (2006), where the singular behavior of the Drucker-Prager yield surface in the zone of the apex is solved by using the multi-surface plasticity theory (following the formulation developed in the work of Sanavia, Steinmann and Schrefler (2002) for isotropic linear hardening/softening and volumetric-deviatoric non-associative plasticity in case of large strain elasto-plasticity). The Drucker-Prager yield function with linear isotropic hardening/softening has been used in the form

$$F(p,\mathbf{s},\xi) = 3\alpha_F p + \|\mathbf{s}\| - \beta_F \sqrt{\tfrac{2}{3}}\,[c_0 + h\xi] \tag{22}$$

in which $p = \frac{1}{3}[\boldsymbol{\sigma}' : \mathbf{1}]$ is the mean effective Cauchy pressure, $\|\mathbf{s}\|$ is the L_2 norm of the deviator effective Cauchy stress tensor $\boldsymbol{\sigma}'$, c_0 is the initial apparent cohesion, α_F and β_F are two material parameters related to the friction angle ϕ of the soil,

$$\alpha_F = 2\frac{\sqrt{\frac{2}{3}}\sin\phi}{3-\sin\phi} \quad \beta_F = \frac{6\cos\phi}{3-\sin\phi} \tag{23}$$

h the hardening/softening modulus and ξ the equivalent plastic strain.

In this paper, the effect of the capillary pressure and temperature on the evolution of the yield surface is not taken into account. The interested reader can refer for example to Alonso, Gens and Josa (1990), Bolzon, Schrefler and Zienkiewicz (1996), Borja (2004) and François and Laloui (2008) for capillary dependent constitutive models in isothermal or non isothermal conditions and to Zhang, Sanavia

and Schrefler (2001) and Zhang, Heeres, de Borst and Schrefler (2001) for the numerical implementation of the constitutive law proposed by Bolzon, Schrefler and Zienkiewicz (1996) (this model has been enhanced by Santagiuliana and Schrefler (2006), where its thermodynamic consistency has been proven).

3.3 Initial and boundary conditions

For the model closure the initial and boundary conditions are needed. The initial conditions specify the full fields of primary state variables at the reference time $t=t_0$, in the whole domain and on its boundary as: $p^g = p_0^g,\ p_c = p_0^c,\ T = T_0,\ \mathbf{u} = \mathbf{u}_0$ on $B \cup \partial B$.

The boundary conditions (BCs) can be of Dirichlet's type on ∂B_π for $t \geq t_0$:

$$p^g = \hat{p}^g \text{ on } \partial B_g, \quad p^c = \hat{p}^c \text{ on } \partial B_c, \quad T = \hat{T} \text{ on } \partial B_T, \quad \mathbf{u} = \hat{\mathbf{u}} \text{ on } \partial B_u \tag{24}$$

or of Cauchy's BCs type on ∂B_π^q for $t \geq t_0$:

$$\begin{aligned}
&[nS_g\rho^{ga}\mathbf{v}^{ga}]\cdot\ \mathbf{n} = q^{ga} \text{ on } \partial B_g^q, \quad c_{wa}\mathbf{v}^{ws}\cdot\ \mathbf{n} = \frac{\hat{p}^{ga}}{K_{ca}}\frac{q^w}{\rho^w} \text{ on } \partial B_c^q,\\
&[nS_g\rho^{gw}\mathbf{v}^{gs} + nS_w\rho^w\mathbf{v}^{ws}]\cdot\ \mathbf{n} = q^{gw} + q^w + \beta_c\left[\rho^{gw} - \rho_\infty^{gw}\right] \text{ on } \partial B_c^q,\\
&[nS_w\rho^w\mathbf{v}^{ws}\Delta H_{vap} - \chi_{eff}grad\,(T)]\cdot\ \mathbf{n} = q^T + \alpha_c\left[T - T_\infty\right] + e\sigma_0\left(T^4 - T_\infty^4\right) \text{ on } \partial B_T^q,\\
&\sigma\cdot\mathbf{n} = \mathbf{t} \text{ on } \partial B_u^q,
\end{aligned} \tag{25}$$

where $\mathbf{v}^{\pi s}(x,t)$ is the π-fluid relative velocity described by the Darcy law, $\mathbf{n}(x,t)$ the unit normal vector, pointing toward the surrounding gas, $q^{ga}(\mathbf{x},t)$, $q^{gw}(\mathbf{x},t)$, $q^w(\mathbf{x},t)$ and $q^T(\mathbf{x},t)$ are the imposed fluxes of dry air, vapor, liquid water and the imposed heat flux, respectively, and $\mathbf{t}(x,t)$ is the imposed traction vector related to the total Cauchy stress tensor $\sigma(\mathbf{x},t)$. $\rho_\infty^{gw}(x,t)$ and $\mathrm{T}_\infty(\mathbf{x},t)$ are the mass concentration of water vapor and the temperature in the far field of undisturbed gas phase, while $\alpha_c(\mathbf{x},t)$ and $\beta_c(\mathbf{x},t)$ are the convective heat and mass exchange coefficients, $e(\mathbf{x},t)$ the emissivity of the interface and σ_o the Stefan-Boltzmann constant.

For the gas boundary conditions, the second of Eq.25 concerns the case when liquid water containing dissolved air at pressure $\hat{p}^{ga}$ enters the boundary∂B_c^q. For the fully saturated state, the initial and boundary conditions for the gas pressure should be formulated by considering the physical meaning of air pressure in the present model, i.e. the variable which describes the dissolved air concentration in pore water with the Henry law, Eq.1, and the assumed relation between these variables, $p^g = p^{ga} + p^{gws}$.

3.4 Numerical solution

The finite element model is derived by applying the Galerkin procedure for the spatial integration and the Generalized Trapezoidal Method for the time integration of the weak form of the balance equations of the previous section [e.g. Lewis and Schrefler (1998), Zienkiewicz, Chan, Pastor, Schrefler, Shiomi (1999)]. In particular, after spatial discretization within the isoparametric formulation, a non-symmetric, non-linear and coupled system of equation is obtained,

$$\begin{bmatrix} \mathbf{C}_{gg} & \mathbf{C}_{gc} & \mathbf{C}_{gt} & \mathbf{C}_{gu} \\ \mathbf{0} & \mathbf{C}_{cc} & \mathbf{C}_{ct} & \mathbf{C}_{cu} \\ \mathbf{0} & \mathbf{C}_{tc} & \mathbf{C}_{tt} & \mathbf{C}_{tu} \\ \mathbf{0} & \mathbf{0} & \mathbf{0} & \mathbf{0} \end{bmatrix} \frac{\partial}{\partial t} \begin{bmatrix} \bar{\mathbf{p}}^g \\ \bar{\mathbf{p}}^c \\ \bar{\mathbf{T}} \\ \bar{\mathbf{u}} \end{bmatrix} + \begin{bmatrix} \mathbf{K}_{gg} & \mathbf{K}_{gc} & \mathbf{K}_{gt} & \mathbf{0} \\ \mathbf{K}_{cg} & \mathbf{K}_{cc} & \mathbf{K}_{ct} & \mathbf{0} \\ \mathbf{K}_{tg} & \mathbf{K}_{tc} & \mathbf{K}_{tt} & \mathbf{0} \\ \mathbf{K}_{ug} & \mathbf{K}_{uc} & \mathbf{K}_{ut} & \mathbf{K}_{uu} \end{bmatrix} \begin{bmatrix} \bar{\mathbf{p}}^g \\ \bar{\mathbf{p}}^c \\ \bar{\mathbf{T}} \\ \bar{\mathbf{u}} \end{bmatrix} = \begin{bmatrix} \mathbf{F}_g \\ \mathbf{F}_c \\ \mathbf{F}_t \\ \mathbf{F}_u \end{bmatrix} \tag{26}$$

where the solid displacements $\mathbf{u}(\mathbf{x},t)$, the capillary and the gas pressure $p^c(\mathbf{x},t)$ and $p^g(\mathbf{x},t)$ and the temperature $T(\mathbf{x},t)$ are expressed in the whole domain by global shape function matrices $\mathbf{N}_u(\mathbf{x})$, $\mathbf{N}_c(\mathbf{x})$, $\mathbf{N}_g(\mathbf{x})$, $\mathbf{N}_T(\mathbf{x})$ and the nodal value vectors $\bar{\mathbf{u}}(t)$, $\bar{\mathbf{p}}^c(t)$, $\bar{\mathbf{p}}^g(t)$, $\bar{\mathbf{T}}(t)$. The elements of the matrices $\mathbf{C}_{ij}$, $\mathbf{K}_{ij}$ and the vectors $\mathbf{F}_i$ are given in the Appendix. In a more concise form the equation system (26) is written as $\mathbf{G}(\mathbf{X}) = \mathbf{C}\frac{\partial \mathbf{X}}{\partial t} + \mathbf{K}\mathbf{X} - \mathbf{F} = \mathbf{0}$, with $\mathbf{X} = \left[\bar{\mathbf{p}}^g, \bar{\mathbf{p}}^c, \bar{\mathbf{T}} \cdot \bar{\mathbf{u}}\right]^T$.

Finite differences in time are used for the solution of the initial value problem over a finite time step $\Delta t = t_{n+1} - t_n$. Following the Generalized Trapezoidal Method equations (26) are rewritten at time $t_{n+\theta}$ using the relationships

$$\left.\frac{\partial \mathbf{X}}{\partial t}\right|_{n+\theta} = \frac{\mathbf{X}_{n+1} - \mathbf{X}_n}{\Delta t},\ \mathbf{X}_{n+\theta} = [1-\theta]\,\mathbf{X}_n + \theta \mathbf{X}_{n+1} \tag{27}$$

with $\theta \in [0,1]$ thus obtaining

$$\mathbf{G}(\mathbf{X}_{n+1}) = [\mathbf{C} + \theta \Delta t \mathbf{K}]|_{n+\theta}\,\mathbf{X}_{n+1} - [\mathbf{C} - (1-\theta)\Delta t \mathbf{K}]|_{n+\theta}\,\mathbf{X}_n - \Delta t \mathbf{F}_{n+\theta} = \mathbf{0} \tag{28}$$

In the computation, fully implicit one-step time integration has been performed ($\theta = 1$).

After time integration, the non-linear system of equation is linearized, thus obtaining the equations system that can be solved numerically (written below in a compact form)

$$\left.\frac{\partial \mathbf{G}}{\partial \mathbf{X}}\right|_{\mathbf{X}^i_{n+1}} \Delta \mathbf{X}^{i+1}_{n+1} \cong -\mathbf{G}\left(\mathbf{X}^i_{n+1}\right) \tag{29}$$

with the symbol $(\bullet)_{n+1}^{i+1}$ to indicate the current iteration (i+1) in the current time step (n+1) and where $\partial \mathbf{G}/\partial \mathbf{X}$ is the Jacobian matrix. Owing to the strong coupling between the mechanical, thermal and the pore fluids fields, a monolithic solution of (29) is preferred using a Newton-Rapson scheme. Finally, the solution vector $\mathbf{X} = \left[\bar{\mathbf{p}}^g, \bar{\mathbf{p}}^c, \bar{\mathbf{T}}, \bar{\mathbf{u}}\right]^T$ is updated by the incremental relationship, $\mathbf{X}_{n+1}^{i+1} = \mathbf{X}_{n+1}^{i} + \Delta \mathbf{X}_{n+1}^{i+1}$.

4 Some remarks on modeling the transition between fully and partially saturated state

The mathematical models of porous media in full and partial saturation, due to the presence of gas phase in the latter condition, contain a different number of equations. For this reason, during modeling of transition between the two states, some theoretical and numerical problems arise. The most correct way, from the theoretical point of view, to deal with this problem is the description of the transition as the so called 'Stefan problem', when two distinct domains, fully and partially saturated with liquid water, are described by different mathematical models and a moving boundary (interface) between them. At the interface some additional conditions (continuity of the state variables, the mass and enthalpy balances) must be fulfilled, see e.g. Nochetto, Paolini and Verdi (1991). The approach is computationally costly, because it needs continuous tracking the actual position of the interface that in the case of 2-D problems and particularly for 3-D ones is time-consuming and rather complicated, Nochetto, Paolini and Verdi (1991). For this reason this approach is very rarely used in practical numerical analyses.

The simplest, from the numerical point of view, and widely used method in practice for modeling fully/partially saturated porous media is the assumption of a 'residual' gas saturation degree (RGSD), S_g^{res}, for the zone fully saturated with liquid water. Hence, the gas phase is present everywhere in the medium and the gas mass balance can be formulated for the whole analyzed domain, even in the 'fully saturated' state, i.e. when $S_w = S_w^{\max} = 1 - S_g^{res}$. The water retention characteristics (e.g. water sorption isotherms) and transport ones (e.g. relative permeability for gas and liquid) should be appropriately modified, $S(p^c, T) \leq S_w^{\max}$, and for $S_w = S_w^{\max}$: $k^{rg} = k_{\min}^{rg} = k^{rg}(S_w^{\max})$, $k^{rw} = k_{\max}^{rw} = k^{rw}(S_w^{\max})$.

The main problem associated with application of the RGSD method, is a proper choice of the S_g^{res} value. This must be small enough to model reasonably 'impermeability' of the saturated material for the gas flow, i.e. to assure possibly small gas mass flux in the saturated zone, in order not to influence significantly the gas pressures in the partially saturated domain. On the other hand, a too small value of the gas saturation degree S_g^{res} can create numerical problems, i.e. ill-conditioning of the equation set, because in such a case the gas permeability will be very low

in the 'saturated' zone, resulting in almost zero values of the terms related to gas pressure gradient in the **K** matrix, Eq.26. For the aforementioned reasons, the S_g^{res} value must be chosen for every considered porous material, usually through numerical experiments ('test and trial' method). It is worth to underline that the RGSD method allows for considering the air dissolved in water, but in a simplified way, i.e. neglecting the mass fluxes of air dissolved in liquid water, Gawin and Sanavia (2010).

Another possibility to solve the 'fully – partially saturated state transition' problem with a numerical technique is the application of a 'switching' procedure (SP) proposed by Gawin and Schrefler (1996), in which the gas mass balance equation is eliminated from the mathematical model. In this method, the physical meaning of capillary pressure is extended to the negative values range, following Pascal's law, which states that the absolute pressure in liquid water equals the pressure exerted by the gas on the free liquid surface (i.e. the atmospheric pressure, $p^g = p_{atm}$) and hydrostatic water pressure (i.e. water pressure respective to the pressure of surrounding gas, p^h), $p^w = p^g + p^h$. Comparing the latter equation to the definition of capillary pressure, $p^c = p^g - p^w$, it is obvious that they coincide, if $p^c = -p^h$. Hence, in the negative values range, p^c means just the water pressure respective to the atmospheric pressure.

The SP method consists in extending the water retention curve (water sorption isotherm) in the range of negative values as follows, $S_w = 1$ for $p^c \leq 0$. If the capillary pressure values in all the nodes of a finite element are negative, the gas pressure value in these nodes is put to the atmospheric pressure value, $p^g = p_{atm}$, what means that the gas mass balance equation is eliminated from the equations set for this element.

Application of the SP method may create some numerical oscillations just after performing the 'switch', when large finite elements or big time steps are used. For this reason, the method requires application of a relatively fine mesh and small time steps during simulations of the transient state. The method was shown to be efficient in analysis of several geotechnical and building physics problems, Gawin and Schrefler (1996), Gawin, Baggio and Schrefler (1996).

Another possibility to analyze the transition between fully and partially saturated state in deformable porous media is the application of the mathematical model proposed in this paper, which can be considered as a kind of a 'physical switching'. It allows for solving the problem in a 'natural way', i.e. without application of any special numerical technique, because the air balance equation, taking into account the air dissolved in liquid water, is valid also in the fully saturated state, Eq.12. The results obtained with the model are the most correct ones, both from the physical and theoretical point of view, of all the aforementioned methods, and the numerical

procedure based on it is more robust than the other ones. This will be shown in the next section, where the methods discussed above are applied.

5 Numerical results

In this section, two examples of desaturation of initially water saturated geomaterials are analyzed with the computer code Comes-Geo [Gawin and Schrefler (1996), Lewis and Schrefler (1998), Sanavia, Pesavento and Schrefler (2006), Gawin and Sanavia (2010)] with appropriate modifications following the mathematical and numerical model presented in Section 3.

The first example simulates the experiment performed by Liakopoulos (1965) concerning outflow of water from a sand column due to gravity force. The second example is based on a plane strain compression test for dense sands where strain localization and cavitation of the pore water were experimentally observed, Mokni and Desrues (1998). These examples will allow us to analyze the effects of dissolved air on the transition from fully to partially saturated state and to compare the results obtained with the four different methods used for modeling such a transition, as described in the previous section. Moreover, the effect of dissolved air on initiation and progress of cavitation at strain localization will be analyzed from a numerical point of view.

5.1 Isothermal drainage of water from a sand column

In the experiment by Liakopoulos (1965), a column of perspex, 1 meter high, was packed by Del Monte sand and instrumented to measure the moisture tension at several points along the column. Before starting the experiment (t<0) water was continuously added from the top and was allowed to drain freely at the bottom through a filter until uniform flow conditions were established. At t=0 the water inflow was ceased. For t>0 the tensiometer readings were recorded and the flow rate at the draining filter was also measured.

The experiment reveals the desaturation of the soil column due to gravitational effects beginning from the top and propagating versus the bottom surface. In fact, negative relative water pressures (i.e. capillary pressure) were measured, developing in time along the column from the top versus the bottom surface. Moreover, the flow rate decreased continuously in time until a very small value was reached.

The experiment is simulated following the numerical benchmark proposed by Gawin and Schrefler (1996) and Gawin, Simoni and Schrefler (1997). The results of this benchmark will be used as reference solution. To simulate this test numerically, the physical properties of the Del Monte sand are necessary. Unfortunately, only the porosity and the hydraulic properties of the sand, i.e. k_w for t<0, $S_w(p^c)$ and

$k^{rw}(p^c)$, were measured by an independent set of experiments, Liakopoulos (1965). The mechanical parameters are those suggested by Gawin and Schrefler (1996) and Gawin, Simoni and Schrefler (1997), where Liakopoulos' test was studied with a non-isothermal two-phase flow model assuming a linear elastic constitutive law for the solid skeleton and isotropic permeability. The material parameters used in the computation are those of Tab. 1. The experimental constitutive laws for $S_w(p^c)$ and $k^{rw}(p^c)$ in isothermal conditions are approximated with the following expressions,

$$S_w = 1 - 0.09680418 \left(\frac{p^c}{p_{ref}} \right)^{2.4279}, \; k^{rw} = 1 - 2.207 \left(1 - S_w\right)^{0.9529} \tag{30}$$

with p_{ref} = 9806 Pa. These relationships are valid for water saturation $S_w \geq 0.91$, as shown by Gawin and Schrefler (1996) and Gawin, Simoni and Schrefler (1997).

The relative permeability of the gas phase, $k^{rg}(p^c)$, was assumed according to the relationship of Brooks and Corey (1966):

$$k^{rg} = (1 - S_e)^2 \left(1 - S_e^{(2+\lambda)/\lambda}\right), \; S_e = (S_w - S_{ir}) / (1 - S_{ir}) \tag{31}$$

where S_e is the effective saturation, S_{ir} the irreducible saturation point and λ the pore size distribution index.

The column is discretized with 20 eight-node isoparametric finite elements of equal size for the solid displacements, temperature, gas pressure and capillary pressure, similarly as in the work of Gawin and Schrefler (1996). Full numerical integration of the discretized spatial domain is selected.

Horizontal displacements are constrained on the lateral surfaces while the bottom surface is also vertically constrained, Fig. 5. Hydrostatic distribution for water pressure (with p^w=9806 Pa at the bottom of the column), gravitational effective stress in the solid skeleton and constant temperature T= 293.15 K are assumed as initial conditions. The initial distribution of gas pressure is assumed to be linear, with p^g= p_{atm} at the top of the column and p^g= (p_{atm} + 9806) [Pa] at its bottom, in order to obtain the initial distribution of dissolved air content corresponding to the maximal solubility of air in water at a given water pressure (it results from this condition that the initial distribution for capillary pressure is p^c = 0, see Section 3.3).

Gravity is considered during the computation, since it is the driving force of the experiment. The lower boundary is drained for t>0, hence water pressure p^w= p_{atm} is assumed, while the other boundaries are impervious.

The problem is solved for four cases, corresponding to the different methods used for modeling the transition between fully and partially saturated states, discussed in Section 4:

Table 1: Material parameters assumed in the first example for the Del Monte sand

Porosity, [-]	0.2975	Solid specific heat, [J/(kg·K)]	810.0
Intrinsic permeability, [m^2]	4.5 10^{-13}	Water viscosity, [Pa·s]	1.0 10^{-3}
Solid grain density, [kg/m^3]	2000.0	Poisson's coefficient, [-]	0.4
Liquid water density, [kg/m^3]	1000.0	Water vapor heat capacity, [J/(kg·K)]	1805.0
Young's modulus, [MPa]	1.3	Water vapor heat conductivity [W/(m·K)]	0.0186
Water heat conductivity, [W/(m·K)]	0.6	Solid cubic thermal expansion coefficient , [K^{-1}]	0.9 10^{-6}
Solid thermal conductivity, [W/(m·K)]	1.442	Solid matrix heat conductivity, [W/(m·K)]	2.5
Irreducible saturation point [-]	0.2	Effective saturation, [-]	0.2
Gravity acceleration [m/s^2]	9.80665	Pore size distribution index [-]	3.0

Case 1: the RGSD method - omitting the air dissolution, with $S_w^{\max}$ =0.9975 at $p^c \leq$ 2175 Pa, k^{rw}= 0 for $S_w \leq S_{ir}$ and k^{rw}= 1.0 for S_w =$S_w^{\max}$, where S_{ir} is the irreducible saturation point.

Case 2: the SP method - omitting the air dissolution, with the numerical switch performed at p^c= 2000 Pa (which corresponds to water degree of saturation S_w = 0.997, Eq.30).

Case 3: the same as case 1, but additionally considering the air dissolution in liquid water in a simplified way, as described by Gawin and Sanavia (2010).

Case 4: the unified approach considering the dissolution of air in liquid water, based on the mathematical model proposed in this paper.

The results of the simulation for case 4, concerning the distributions of capillary pressure, gas pressure and water saturation degree along the column height, are plotted at different time stations in Fig. 6a-8a and compared in Fig. 6b-8b and 6c-8c to the results obtained for other cases at time stations t=10 min and t=120 min, accordingly. The vertical displacements for the four cases are compared in Fig. 9 at the time station t=5 min; the small variation observed in this figure disappears for advanced stages of the process.

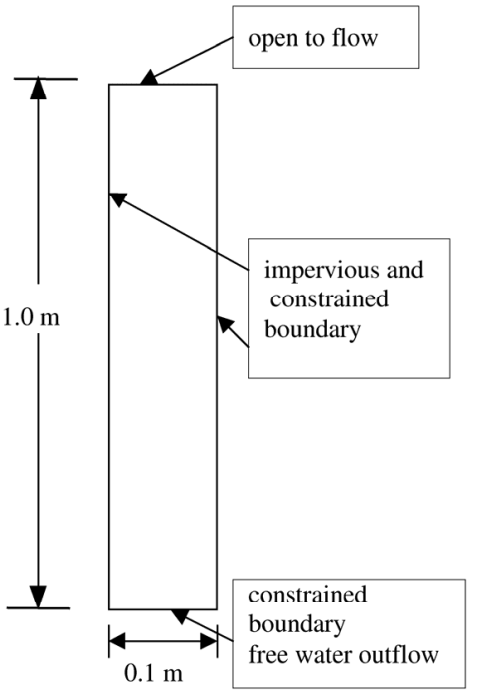

Figure 5: Scheme of Liakopoulos' test, Liakopoulos (1965)

The time histories of the outflow rate of liquid water at the bottom surface (Darcy's velocity along the vertical direction of the left nodal point of the bottom) for all the cases are very similar and are not depicted here.

From figures 6-9, one can observe that the release of air dissolved in liquid water has small influence on displacements (and outflow), but not for gas pressure, capillary pressure and for saturation, mainly on the onset. Of course, one should keep in mind that the maximum saturation degree for the cases 1 and 3, due to application of the RGDS method, is slightly smaller than one.

Some more distinct differences can be noticed for the capillary pressure and gas pressure profiles, especially at the initial stages of the process, when the released air causes an increase of gas pressure (Fig. 7b) and slightly higher values of capillary pressures (Fig. 6b), what results in faster desaturation (compare the cases 1 and 3 at Fig. 8b). The solutions obtained with the considered methods do not differ significantly, especially those of the cases 3 and 4, which are practically the same with exception of the saturation profiles (due to different $S_w^{\max}$ value). The capillary

pressure profiles for these cases reveal the same character as those for the case 2, i.e. existence of a zone with capillary pressure value which remains almost constant. This shows that the shape of capillary pressure profiles for case 2 is of physical origin, and not just result of the numerical 'switching' procedure.

The results of our simulations are compared with those of Vaunat, Gens and Jommi (1997) in the Fig. 6b-c, 7b-c and 8b-c. Different time history profiles, labeled VGJ07, can be observed, which reveal a smaller influence of the air released on capillary pressure, gas pressure and water saturation than that we have described with our models, especially in the lower $3/4$ of the column. Moreover our models have not captured the saturation front, (see Fig. 8b-c), which splits the column into a saturated part and an unsaturated part. A possible explanation could be the assumed negligible effect of the solid velocity in the mass balance equations by Vaunat, Gens and Jommi (1997), which is related to the volumetric deformations and the use of a null value for the min k^{rg} , Jommi, Vaunat, Gens, Schrefler and Gawin (1997) (the value of 10^{-4} is used in this work for cases 1-4 when $p^c < 10^{-4}$ Pa).

The analyzed numerical techniques for modeling the transition between fully and partially saturated states of porous materials, i.e. the RGSD (case 1) and SP (case 2) methods, even if they are based on the simplified physical models of the process, have given results which are in a reasonable agreement with the more sophisticated mathematical models, like those proposed here (case 4) and by Gawin and Sanavia (2010), (case 3).

To analyze more in detail the effects of air dissolution and its further release from liquid pore water on the process evolution, dealt here with the full (case 4) and simplified (case 3) models, the space distributions of dissolved air concentration in liquid water at different time stations are presented for case 4 in Fig. 10a. The results for the two analyzed cases are compared at time stations t= 1, 5, 10 and 120 min in Fig. 10b. As can be observed, the highest mass of air (about 0.75 g/m^3, corresponding to about 0.58 l/m^3 at atmospheric pressure) is released, especially at the initial stages of the process, from the liquid water close to the column bottom, where the most rapid decrease of the dissolved air pressure occurs. Moreover, there is almost no difference between the results obtained with the two analyzed methods (cases 3 and 4), Fig. 10b.

The time evolutions of the mass fluxes of gas phase and air dissolved in liquid water, together with the changes of water saturation degree, are shown in Fig. 11, for two points at different height, h=0.5 m, in the middle of the column, and h= 0.9 m, close to its top surface. The negative values correspond to the fluxes flowing towards the bottom of the column. At the first height (h= 0.9 m), where the sand starts desaturation immediately, the dissolved air flux in liquid water is much smaller than

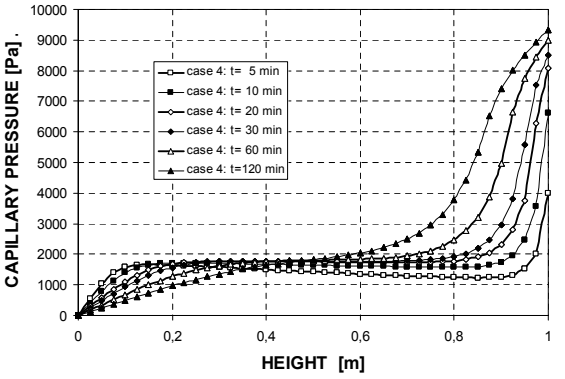

a

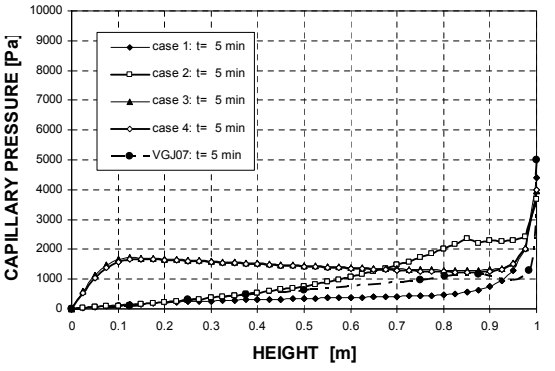

b

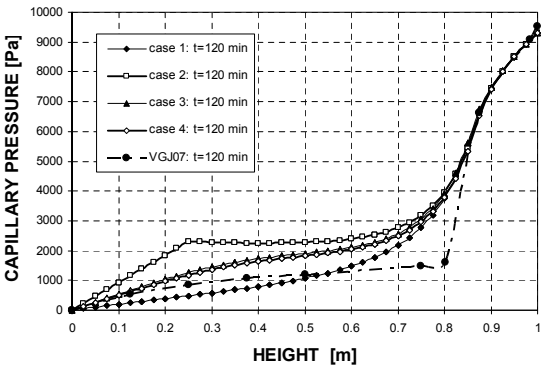

c

Figure 6: The simulated capillary pressure profiles at different time stations during the Liakopoulos test: a) results obtained with the model considering the effects of the air dissolved in pore water (case 4), b) comparison of the results obtained with 4 different methods at time station t= 5 min, c) comparison of the results obtained with 4 different methods at time station t= 120 min

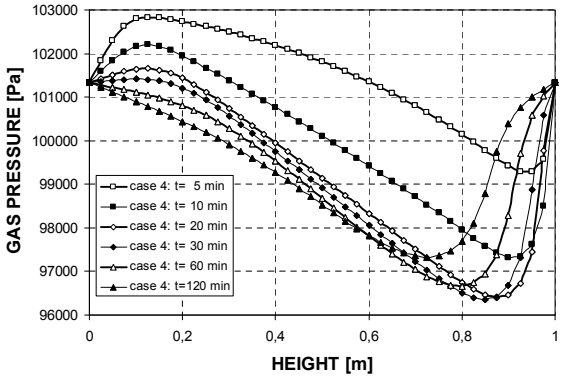

a

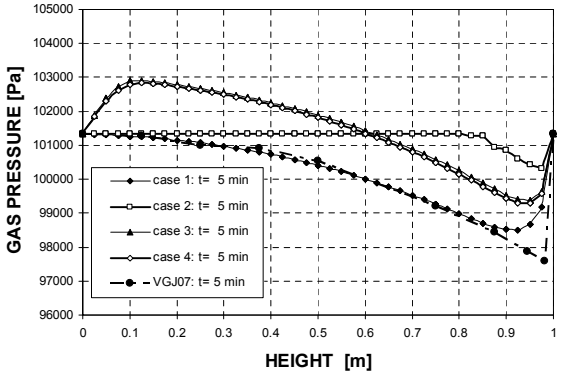

b

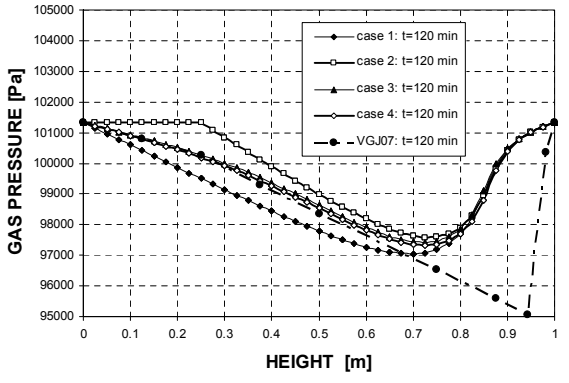

c

Figure 7: The simulated gas pressure profiles at different time stations during the Liakopoulos test: a) results obtained with the model considering the effects of the air dissolved in pore water (case 4), b) comparison of the results obtained with 4 different methods at time station t= 5 min, c) comparison of the results obtained with 4 different methods at time station t= 120 min.

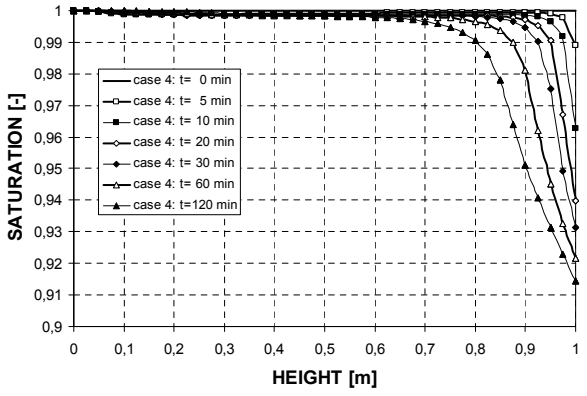

a

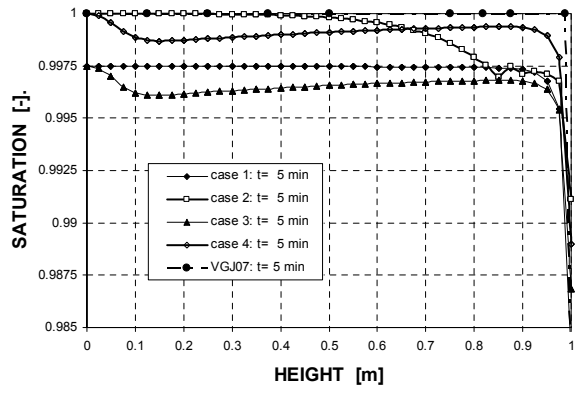

b

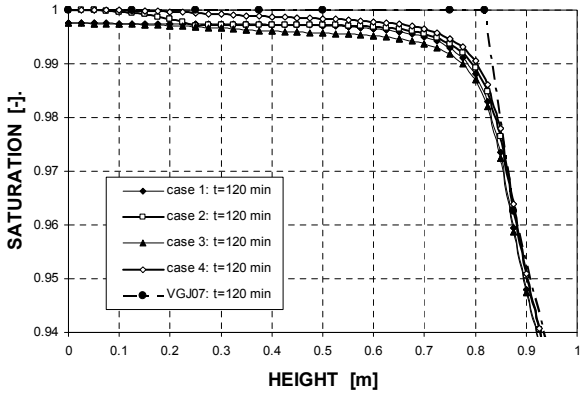

c

Figure 8: The simulated saturation degree profiles at different time stations during the Liakopoulos test: a) results obtained with the model considering the effects of the air dissolved in pore water (case 4), b) comparison of the results obtained with 4 different methods at time station t= 5 min, c) comparison of the results obtained with 4 different methods at time station t= 120 min

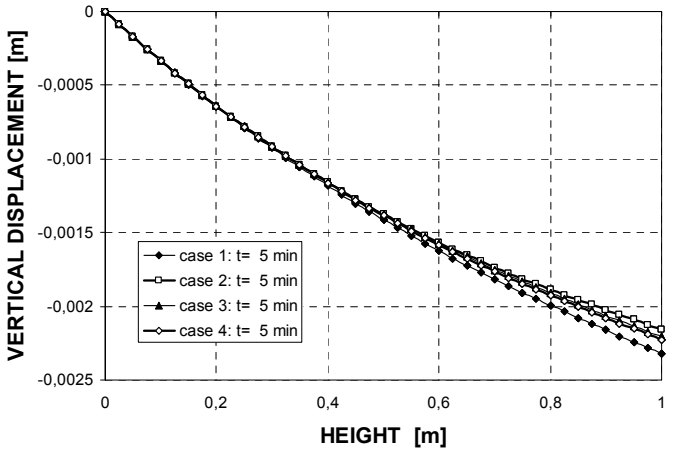

Figure 9: The simulated vertical displacement profiles during the Liakopoulos test: comparison of the results obtained with 4 different methods at time station t= 5 min

that in the gas phase, and it is considerable only during the first 2 hours, Fig. 11b. At the second position (h=0.5 m), where the process is much slower and the saturation degree remains very high all the time, the dissolved air flux is initially even higher than that in the gas phase, and then it decreases gradually, becoming insignificant after about 10 hours, as can be seen in Fig. 11a. This shows that the mass flux of air dissolved in liquid water can be considerable and plays an important role in the gas mass transport in porous media at very high water saturation degrees (see also Fig. 8b). Moreover, thanks to this effect, the terms related to the air accumulation and transport in the matrices **C** and **K**, (see Eq.26 and Appendix), have values high enough to improve visibly numerical performance of the computer code.

5.2 Isothermal plane strain compression test of a dense sand

This example deals with the simulation of a plane strain compression test of undrained water saturated dense sand, where strain localization and cavitation of the liquid pore water were experimentally observed, Mokni and Desrues (1998). This process was already analyzed numerically by Sanavia, Pesavento and Schrefler (2006) without considering the air dissolved in liquid water and by Gawin and Sanavia (2010) with the simplified model for dissolved air. Here the example is simulated with the same four methods as in Section 5.1 (cases 1-4), but with $S_w^{\max} = 0.9965$ for cases 1 (RGSD method) and 3 (a greater value was not possible because of ill conditioning of the Jacobian matrix of Eq.29 for case 3).

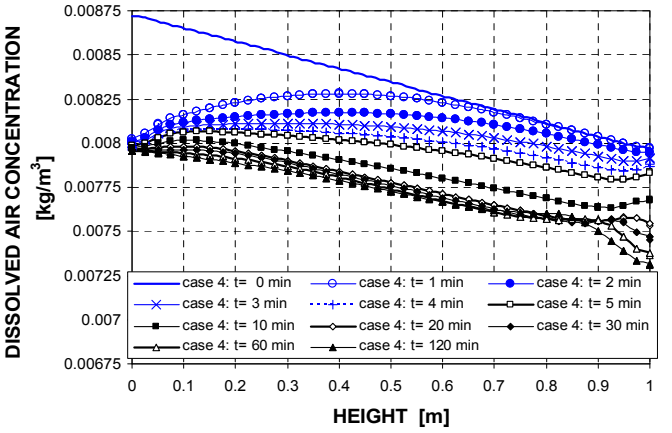

a

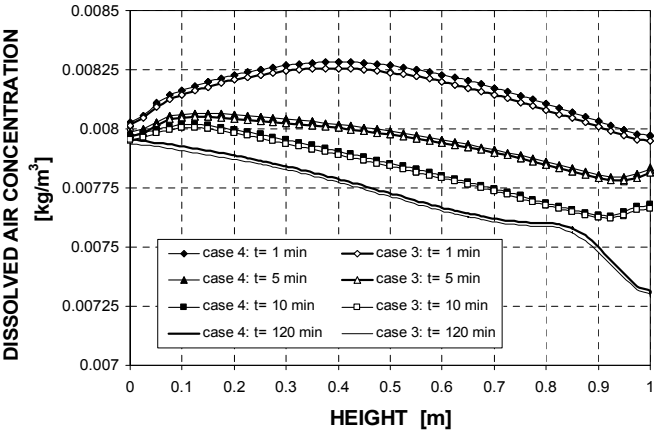

b

Figure 10: The simulated dissolved air concentrations profiles at different time stations during the Liakopoulos test: a) results obtained with the model considering the effects of the air dissolved in pore water (case 4), b) comparison of the results obtained for the cases 3 and 4 at time station t= 1, 5, 10 and 120 min

The rectangular sample of homogeneous soil of 34 cm height and 10 cm width has been discretized using a regular mesh of 340 (34x10) isoparametric quadrilateral 8-node elements, Fig. 12. The material is initially fully saturated with liquid water and the boundaries of the sample are impervious and adiabatic. Imposed vertical displacements are applied on the top surface with the constant rate of 1.2 mm/s until strain localization has been observed. Vertical and horizontal displacements are

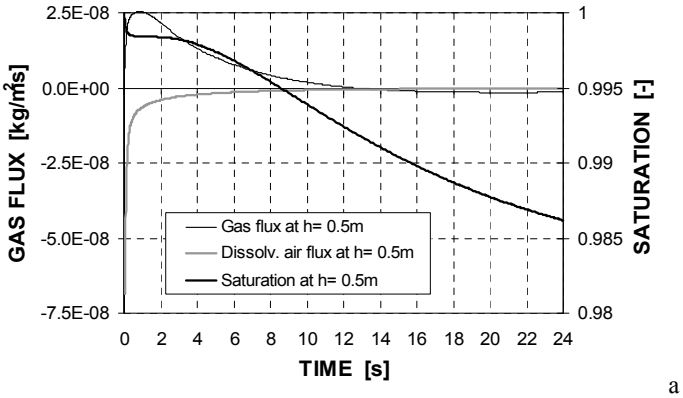

a

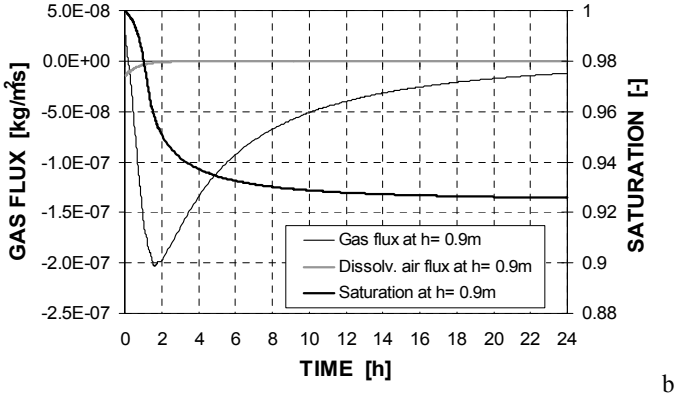

b

Figure 11: The time evolutions of mass fluxes of gas phase and air dissolved in liquid water, and changes of water saturation degree during the Liakopoulos experiment at two different heights: a) h= 0.5m, b) h= 0.9 m

constrained at the bottom surface. Plane strains and quasi-static loading conditions are assumed.

The initial temperature in the sample is constant and fixed at the ambient value. The initial distribution of gas pressure is assumed to be linear, with $p^g = p_{atm}$ at the top of the column and $p^g = (p_{atm} + 3334)$ [Pa] at its bottom, in order to obtain the initial distribution of dissolved air content corresponding to the maximal solubility of air in water at a given pressure. Gravity forces are taken into account. The mechanical behavior of the solid skeleton is simulated by using the elasto-plastic Drucker-Prager constitutive model, with isotropic linear softening behavior as phenomenological description of damage effects and non associated plastic flow. The

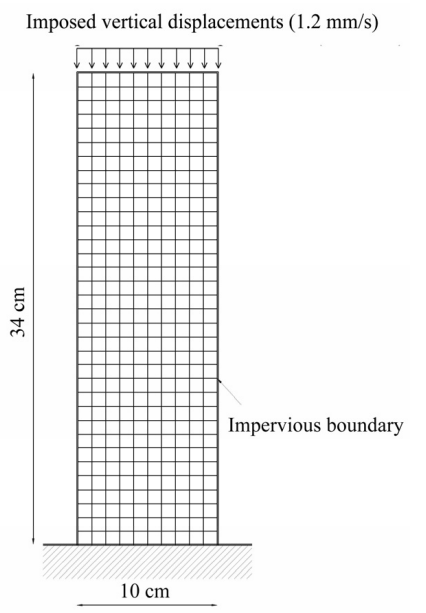

Figure 12: Geometry and boundary conditions for the second numerical example

material parameters used in the computation are listed in Tab. 2, the same as in Sanavia, Pesavento and Schrefler (2006) and Gawin and Sanavia (2010) for sake of comparison.

The constitutive relationships for the water degree of saturation $S_w(p^c)$ and water relative permeability $k^{rw}(S_w)$ are of Safai and Pinder (1979) in isothermal conditions. For the gas relative permeability $k^{rg}(S_w)$, the relationship of Brooks and Corey (1966) in isothermal conditions has been assumed. These relationships have been used because of lack of experimental data.

In the finite element analysis, the dilatant behavior of dense sands is simulated selecting a positive value of the angle of dilatancy (20°). For this material in undrained conditions, the increment of the void ratio due to the volumetric plastic deformations causes a drop of the water pressure if liquid water is not supplied. As a result, cavitation develops if water pressure lower than or equal to the saturation vapor pressure at the temperature of the sample is reached (p^{gws}= 2338.8 Pa).

The results of the computation in the entire domain for case 4 for the variables volumetric strain, vapor pressure and total released air are plotted at the end of the simulation in Fig. 13-15, respectively (the same results for case 2 are presented in

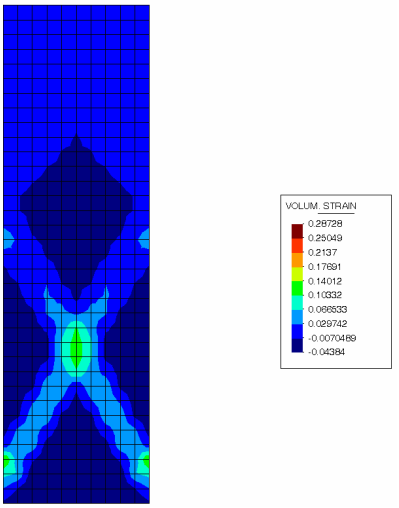

Figure 13: Volumetric strain [-] contour obtained at the end of the numerical simulation (t= 29.4 s) and position of the nodal point of the Fig. 16-18

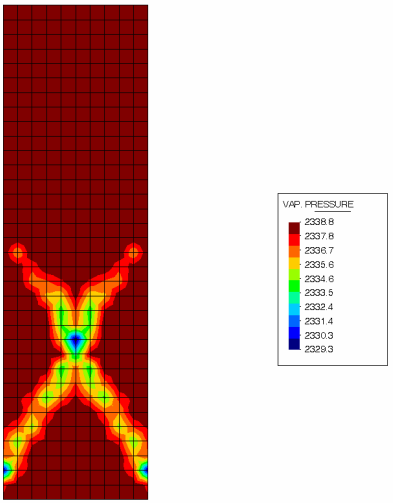

Figure 14: Vapor pressure [Pa] contour obtained at the end of the numerical simulation (t= 29.4 s)

the work of Sanavia, Pesavento, Schrefler (2006), while the ones for cases 1 and 3 in Gawin and Sanavia (2010). Comparison of the results of the four cases is plotted in Fig. 16-18 by means of time histories in the nodal point 331 inside the shear bands (the position of this point is indicated in Fig. 13).

For the analyzed cases, the numerical results indicate the pronounced accumulation of inelastic strains in narrow zones. Because of the dilatant behavior of the shear bands, positive volumetric strains develop inside the plastic zones, while the negative values are observed in the elastic domain (Fig. 13). As a consequence, water pressure decreases inside the plastic zones up to the development of capillary pressures, as depicted in Fig. 17a. At these conditions a vapor phase appears (i.e. water cavitation starts) because the water pressure decreases below the saturation vapor pressure at ambient temperature of 2338.8 Pa (see Fig. 14 and Fig. 17b) and a gradual water desaturation in the strain localization bands initiates (Fig. 16b). Cavitation of water is hence described directly by the model, as shown in Fig. 14 and 17b; in particular, in Fig. 14 can be observed that the vapor phase appears only inside the dilatant plastic zones (in the model, vapor pressure equal to the saturation values, $p^{gw} = p^{gws}$, means relative humidity equal to 100%RH and full saturation with water, while $p^{gw} < p^{gws}$ means partial saturation). At the same time, the shear bands become partially saturated, as it can be seen in Fig. 16b.

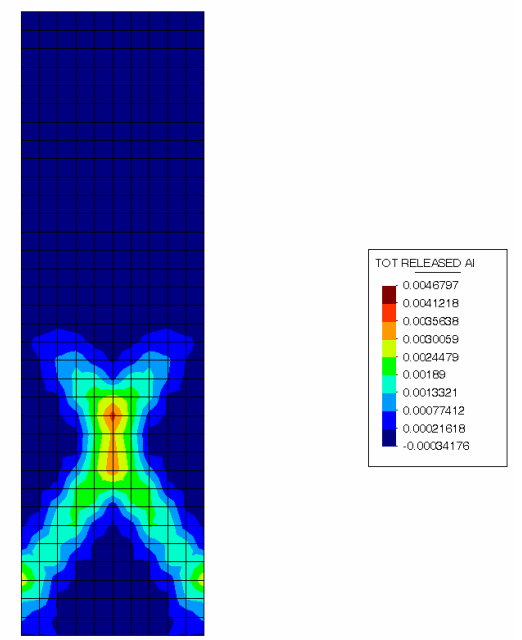

Figure 15: Contour of total amount of dissolved air released from the pore water [kg/m^3], obtained at the end of the numerical simulation (t= 29.4 s)

The comparison between the solutions of the four models, Fig. 16-18, shows that the numerical results are very similar for all cases, with exception of case 3. The differences between case 3 and 4 are due to the assumption that model 3 neglects the dissolved air advection, which is related to the water pressure gradients that are significant for the analyzed example. Moreover, these differences are due also to the different modeling of the air release, dependent on the water pressure for case 3 and on the air pressure for case 4. As can be observed in Fig. 18, the time instants when water and gas pressures start to decrease are shifted in time, causing considerable difference for the time of cavitation initiation. These differences can be also explained by analyzing Fig. 18b, where the released air mass in time is depicted. In fact, it can be observed that the released air is visibly accelerated for case 3, in comparison with case 4.

Only for the vapor pressure (Fig. 17b) a small difference between the cases 4 and 1-2 can be observed, because the release of air accelerates slightly the initiation of cavitation, while the contribution of the air released is considerable for case 3. Unfortunately, from the experimental point of view, the influence of air dissolved on the onset and further progress of cavitation during strain localization is unknown

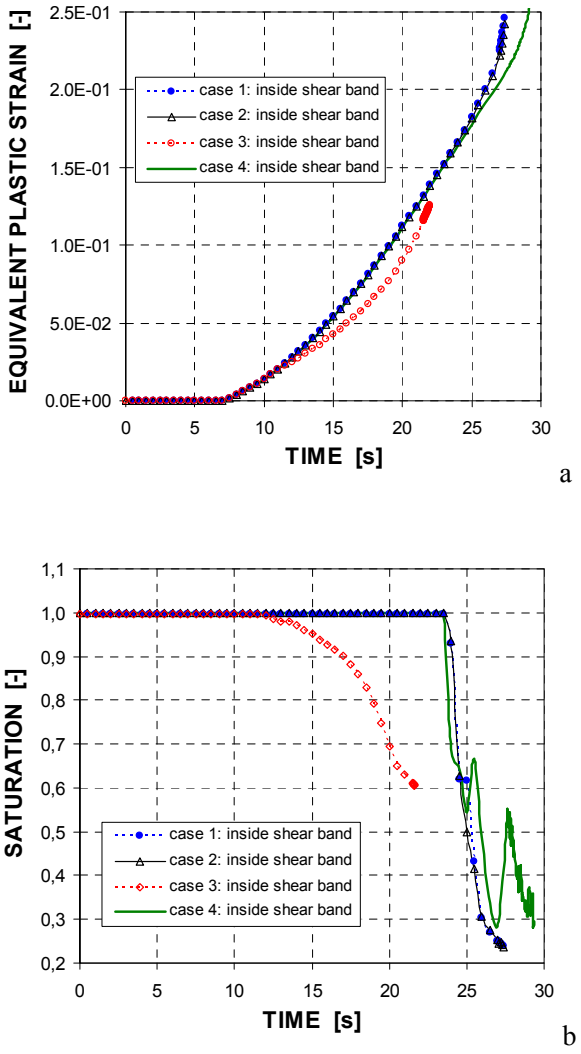

Figure 16: Comparison of the numerical simulation results in the point inside the strain localization band, obtained with the four models: a) Equivalent plastic strain vs. time, b) Saturation degree vs. time.

to the authors' knowledge, so the model developed in this work and the more simplified one by Gawin and Sanavia (2010) cannot be validated for the aspect we are dealing with.

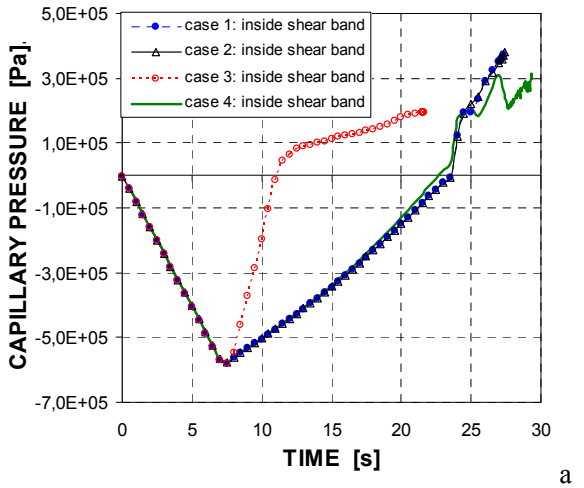

a

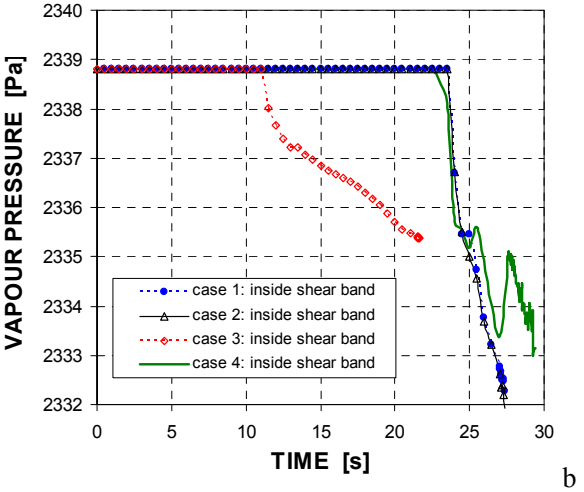

b

Figure 17: Comparison of the numerical simulation results in the point inside the strain localization band, obtained with the four models: a) Capillary pressure vs. time, b) Vapor pressure vs. time

As far as regularization properties of the multiphase models in case of strain localization are concerned, the interested reader is referred to, e.g., Ehlers and Volk (1999), Zhang, Sanavia and Schrefler (1999), Schrefler, Zhang and Sanavia (1999), Benallal and Comi (2004), Abellan and de Borst (2006), Schrefler, Zhang and Sanavia (2006) and Zhang, Qin, Sanavia and Schrefler (2007). Here, the shear

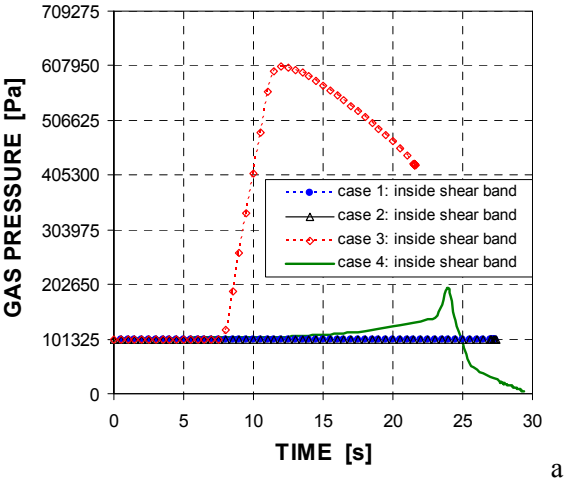

a

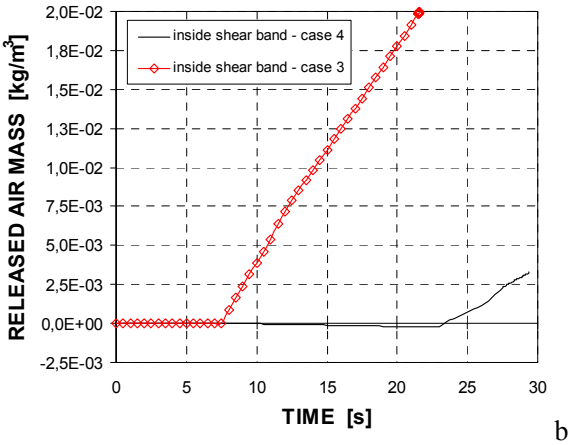

b

Figure 18: Comparison of the numerical simulation results in the point inside the strain localization band: a) Gas pressure vs. time, obtained with the four models, b) Released air mass vs. time, obtained with two models

band width is fixed by the element size, which was selected close to the experimental band width of Mokni and Desrues (1998).

6 Conclusions

A coupled mathematical model for the hydro-thermo-mechanical behavior of saturated and partially saturated porous media was extended to consider the effects

Table 2: Material parameters assumed in the second example for dense sand

Porosity, [-]	0.2	Solid specific heat, [J/(kg·K)]	810.0
Intrinsic permeability, [m^2]	$1.0\ 10^{-14}$	Water viscosity, [Pa·s]	$1.0\ 10^{-3}$
Solid grain density, [kg/m^3]	2000.0	Water heat conductivity, [W/(m·K)]	0.6
Liquid water density, [kg/m^3]	1000.0	Water vapor heat capacity, [J/(kg·K)]	1805.0
Young's modulus, [MPa]	30.0	Poisson's coefficient, [-]	0.4
Water vapor heat conductivity, [W/(m·K)]	0.0186	Solid cubic thermal expansion coefficient , [K^{-1}]	$0.9\ 10^{-4}$
Solid thermal conductivity, [W/(m·K)]	1.442	Solid matrix heat conductivity, [W/(m·K)]	2.5
Irreducible saturation point [-]	0.2	Effective saturation, [-]	0.2
Gravity acceleration [m/s^2]	9.80665	Pore size distribution index [-]	3.0
Cohesion in water saturated conditions, [MPa]	0.5	Plastic modulus, [MPa]	-1.0
Internal friction angle, [deg]	30°	Dilatancy angle, [deg]	20°

of air dissolved in liquid water. Physics of air dissolution and water cavitation in porous media, as well as different numerical techniques used for modeling the transition between fully and partially saturated state, were briefly discussed. Finite element solution of the model equations were used to analyze two examples.

It was shown that considering the effect of the dissolved air released from liquid water upon the progress of physical phenomena during the transition from fully to partially saturated state has a small influence on overall results of numerical simulations both for water outflow due to gravity forces (Liakopoulos test) and the fluid flows and cavitation accompanying water desaturation in the strain localization zones during compression test of undrained dense sand. There are, however, significant differences for the fluids variables, visible only in a limited time/space domain, where the rate of pressure changes and the released mass and flux of dissolved air are considerable. From this point of view, the dissolved air can be ne-

glected in most practical applications, and the results obtained are still of sufficient accuracy, unless very particular time dependent processes where air dissolution could play a role need to be simulated. This is, for example, the case reported by LeBihan and Leroueil (2002) to describe the unexpected pore pressures observed in the core of some earth dams.

The dissolved air formulation may be important if appropriate constitutive models for partially saturated materials are used. Further, considering properly air dissolution in the hydro-thermo-mechanical formulation allows for a unified modeling of partially and fully saturated media, without application of any 'unphysical' numerical techniques necessary to assure a good numerical performance of computer codes which do not take into account the air dissolution.

Acknowledgement: The authors would like to thank the University of Padua, Italy, (research grants *STPD08JA32* and *CPDA097373*) for the financial support. This research was developed within the framework of ALERT Geomaterials Association (http://alert.epfl.ch).

References

Abellan, M.A.; de Borst, R. (2006): Wave propagation and localisation in a softening two-phase medium. *Computer Methods in Applied Mechanics and Engineering*, vol. 195, pp. 5011-5019.

Alonso, E.E., Gens, A.; Josa, A. (1990): A constitutive model for partially saturated soils. *Géotechnique*, vol. 40, pp. 403-430.

Atkins, P.; de Paula, J. (2002): *Atkins' Physical Chemistry*. Seventh Edition, Oxford University Press, New York.

Benallal, A.; Comi, C. (2003): On numerical analysis in the presence of unstable saturated porous materials. *Int. J. Numer. Meth. Engng.*, vol. 56, pp. 883–910.

Bolzon, G.; Schrefler, B.A.; Zienkiewicz, O.C. (1996): Elastoplastic soil constitutive laws generalized to partially saturated states. *Géotechnique,* vol.46, pp. 279-289.

Borja, R. I. (2004): Cam-Clay plasticity. Part V: A mathematical framework for three-phase deformation and strain localization analyses of partially saturated porous media. *Computer Methods in Applied Mechanics and Engineering*, vol. 193, pp. 5301-5338.

Brooks, R.N.; Corey, A.T. (1966): Properties of porous media affecting fluid flow. *Journal of Irrigation Drain. Division of the American Society of Civil Engineering*. 92(IR2), pp. 61-68.

Collin, F.; Li, X.L.; Radu, J.P.; Charlier R. (2002): Thermo-Hydro-Mechanical Coupling in clay barriers, *Engineering Geology*, vol. 64, pp. 179-193.

Coussy, O. (2004): *Poromechanics*. J. Wiley & Sons, Ltd.

de Boer, R. (2000): Theory of Porous Media: Highlight in Historical Development and Current State. Springer-Verlag, Berlin.

Ehlers, W.; Volk, W. (1997): On shear band localization phenomena of liquid-saturated granular elastoplastic porous solid materials accounting for fluid viscosity and micropolar solid rotations. *Mechanics Cohesive-Frictional Materials and Structures,* vol. 2, pp. 301-320.

Ehlers, W.; Graf, T.; Ammann, M. (2004): Deformation and localization analysis of partially saturated soil, *Computer Methods in Applied Mechanics and Engineering,* vol. 193, pp. 2885-2910.

Ferguson, W.J.; Palananthakumar, B. (2005): A fully coupled finite element model of landfill gas mitigation in a partially saturated soil. *CMES: Computer Modeling in Engineering & Sciences*, vol. 8, pp. 201-216.

François, B.; Laloui, L. (2008): ACMEG-TS: a constitutive model for unsaturated soils under non-isothermal conditions. *Int. J. Numer. Anal. Meth. Geomech.* DOI: 10.1002/nag.712

Gawin, D.; Schrefler, B.A. (1996): Thermo-hydro- mechanical analysis of partially saturated porous materials. *Engineering Computations*, vol. 13(7), pp. 113-143.

Gawin, D.; Sanavia, L. (2010): Simulation of cavitation in water saturated porous media considering effects of dissolved air, *Transport in porous media,* vol. 81(1), pp. 141-160. DOI: 10.1007/s11242-009-9391-4

Gawin, D.; Baggio, P.; Schrefler, B.A. (1996): Modelling heat and moisture transfer in deformable porous building materials. *Archives of Civil Engineering*, vol. 42(3), pp. 325-349.

Gawin, D.; Simoni, L.; Schrefler, B.A. (1997): Numerical model for hydro-mechanical behaviour in deformable porous media: a benchmark problem. In: Jian-Xin Yuan (eds) *Computer methods and advances in Geomechanics*. Vol. 2, Balkema, Rotterdam, pp. 1143-1148.

Gawin, D.; Sanavia, L.; Schrefler, B.A. (1998): Cavitation modelling in saturated geomaterials with application to dynamic strain localization. *Int. J. Num. Meth. Fluids.,* vol. 27, pp. 109-125.

Gens, A.; Garcia-Molina, A.J.; Olivella, S.; Alonso, E.E.; Huertas, F. (1998): Analysis of a full scale in situ test simulating repository conditions. *Int. J. Numer. Anal. Meth. Geomech*., vol. 22, pp. 515-548.

Gens, A.; Olivella, S. (2000): Non isothermal multiphase flow in deformable porous media. Coupled formulation and application to nuclear waste disposal, in *Developments in Theoretical Geomechanics,* Smith and Cartes (Eds), Balkema, Rotterdam.

Gens, A.; Olivella, S. (2001): THM phenomena in saturated and unsaturated porous media. Fundamentals and formulation. *Revue française de genie civil*, vol. 5, pp. 693-717.

Gerard, P.; Charlier, R.; Barnichon, J.-D.; Su, K.; Shao, J.-F.; Duveau, G.; Giot, R.; Chavant, C.; Collin, F. (2008): Numerical modelling of coupled mechanics and gas transfer around radioactive waste in long-term storage: *Journal of Theoretical and Applied Mechanics,* vol. 1-2, pp. 25-44.

Gray, W.G.; Hassanizadeh, M. (1991): Unsaturated flow theory including interfacial phenomena. *Water Resources Research*, vol. 27,(8), pp. 1855-1863.

Hassanizadeh, M.; Gray, W.G. (1979a): General conservation equations for multiphase system: 1. Averaging technique. *Adv. Water Res.,* vol. 2, pp. 131-144.

Hassanizadeh, M.; Gray, W.G. (1979b): General conservation Equations for multi-phase system: 2. Mass, momenta, energy and entropy equations. *Adv. Water Res.,* vol. 2, pp. 191-201.

Hassanizadeh, M.; Gray, W.G. (1980): General conservation equations for multiphase system: 3. Constitutive theory for porous media flow. *Adv. Water Res.,* vol. 3, pp. 25-40.

Jabbari, E. Gatmiri, B. (2007): Thermo-Poro-Elastostatic Green's Functions for Unsaturated Soils. *CMES: Computer Modeling in Engineering & Sciences*, vol. 18, pp. 31-44.

Jommi, C.; Vaunat, J.; Gens, A.; Schrefler, B.A.; Gawin, D. (1997): Multiphase flow in porous media: a numerical benchmark. Proc. NAFEMS World Congress, Stuttgart (D), Vol. 2, pp. 1338-1349.

Khalili, N.; Loret, B.; (2001): An Elasto-Plastic Model for non-isothermal analysis of flow and deformation in unsaturated porous media: formulation. *Int. J. Solids and Structures,* vol. 38, pp. 8305-8330.

LeBihan, J.P.; Leroueil, S. (2002): A model for gas and water flow through the core of earth dams, *Canadian Geotechnical Journal,* vol. 39(1), pp. 90-102.

Lewis, R.W.; Schrefler, B.A. (1998): *The Finite Element Method in the Static and Dynamic Deformation and Consolidation of Porous Media*. John Wiley & Sons, Chichester.

Liakopoulos, A.C. (1965): Transient flow through unsaturated porous media, PhD thesis, University of California, Berkeley (CA), USA

Maris, H.; Balibar, S. (2000): Negative pressures and cavitation in liquid Helium, *Physics Today,* vol. 53(2), pp. 29-34.

McManus, K.J.; Davis, R.O. (1997): Dilatation induced pore fluid cavitation in sands, *Géotechnique,* vol. 47(1), pp. 173-177.

Mercury, L.; Azaroual, M.; Zeyen, H.; Tardy, Y. (2003): Thermodynamic properties of solutions in metastable systems under negative or positive pressures. *Geochimica et Cosmochimica Acta,* vol. 67(10), pp. 1769-1785.

Mokni, M.; Desrues, J. (1998): Strain localisation measurements in undrained plane-strain biaxial tests on Hostun RF sand. *Mechanics of Cohesive-Frictional Materials,* vol. 4, pp. 419-441.

Nochetto, R.H.; Paolini, M.; Verdi, C. (1991): An adaptive finite element method for two-phase Stefan problems in two space variables. *Math Comput.*, pp. 78–108.

Olivella, S.; Carrera, J.; Gens, A.; Alonso, E.E. (1994): Nonisothermal multiphase flow of brine and gas through saline media. *Transport in Porous Media*, vol. 15, pp. 271-293.

Or, D.; Tuller, M. (2002): Cavitation during desaturation of porous media under tension. *Water Resources Research,* vol. 38(5), pp. 1061-1064.

Safai, N.M.; Pinder, G.F. (1979): Vertical and horizontal land deformation in a desaturating porous medium. *Advances in Water Resources*, vol. 2, 19-25

Sanavia, L.; Schrefler, B.A.; Steinmann, P. (2002): A formulation for an unsaturated porous medium undergoing large inelastic strains. *Computational Mechanics,* vol. 28, pp. 137-151.

Sanavia, L.; Pesavento, F.; Schrefler, B.A. (2006): Finite element analysis of non-isothermal multiphase geomaterials with application to strain localization simulation. *Computational Mechanics,* vol. 37(4), pp. 331-348.

Santagiuliana R.; Schrefler, B.A. (2006): Enhancing the Bolzon-Schrefler-Zienkiewicz Constitutive Model For Partially Saturate Soil. *Transport in Porous Media,* vol. 65, pp. 1-30.

Schrefler, B.A. (1984): *The Finite Element Method in Soil Consolidation (with applications to Surface Subsidence).* PhD. Thesis, University College of Swansea, C/Ph/76/84, Swansea UK.

Schrefler, B.A. (2002): Mechanics and Thermodynamics of Saturated-Unsaturated Porous Materials and Quantitative Solutions. *Applied Mechanics Review,* vol. 55, pp. 351-388.

Schrefler, B.A.; Gawin, D. (1996): The effective stress principle: incremental or finite form?, *Int. J. Numer. Anal. Meth. Geomech.*, vol. 20(11), pp. 785-815.

Schrefler, B.A.; Sanavia, L.; Majorana, C.E. (1996): A multiphase medium model for localisation and postlocalisation simulation in geomaterials. *Mechanics of Cohesive-Frictional Materials,* vol. 1, pp. 95-114.

Schrefler, B.A.; Zhang, H.W.; Sanavia, L. (1999): Fluid-structure interaction in the localisation of Saturated porous media. *ZAMM Zeitschrift für Angewandte Mathematik und Mechanik (Journal of Applied Mathematics and Mechanics)*, vol. 79(7), pp. 481-484.

Schrefler, B.A.; Zhang, H.W.; Sanavia, L. (2006): Interaction between different internal length scales in fully and partially saturated porous media - the 1-D case. *Int. J. for Numerical and Analytical Methods in Geomechanics*, vol. 30, pp. 45-70.

Selvadurai, A.P.S.; Ghiabi, H. (2008): Consolidation of a Soft Clay Composite: Experimental Results and Computational Estimates. *CMES: Computer Modeling in Engineering & Sciences*, vol. 23, pp. 53-74.

Thomas, H.R.; He, Y.; Sansom, M.R.; Li, C.L.W. (1994): On the development of a model of the thermo-mechanical-hydraulic behaviour of unsaturated soils, *Engineering Geology,* vol. 41, pp. 197-218.

Tyree, M.T. (1997): The Cohesion-Tension theory of sap ascent: current controversies. *Journal of Experimental Botany,* vol. 48(315), pp. 1753-1765.

Vardoulakis, I.; Sulem, J. (1995): *Bifurcation Analysis in Geomechanics*. Blackie Academic & Professional.

Vaunat, J.; Gens, A.; Jommi, C. (1997): A strategy for numerical analysis of the transition between saturated and unsaturated flow conditions. Numerical Models in Geomechanics, Pietruszczak & Pande (eds), Balkema, Rotterdam, pp. 297-302.

Zhang, H.W.; Sanavia, L.; Schrefler, B.A. (1999): An internal length scale in dynamic strain localisation of multiphase porous media, *Mechanics of Cohesive-Frictional Materials*, vol. 4, pp. 443-460

Zhang, H.W.; Sanavia, L.; Schrefler, B.A. (2001): Numerical analysis of dynamic strain localisation in initially water saturated dense sand with a modified generalised plasticity model, *Computers and Structures,* vol. 79, pp. 441-459.

Zhang, H.W.; Heeres, O.M.; de Borst, R.; Schrefler, B.A. (2001): Implicit integration of a generalized plasticity constitutive model for partially saturated soil, *Engineering Computations*, vol. 18, pp. 314-336.

Zhang, H.W.; Qin, J.M.; Sanavia, L.; Schrefler, B.A. (2007): Some theoretical aspects of strain localization analysis of multiphase porous media with regularized constitutive models. *Mechanics of Advanced Materials and Structures*, vol. 14(2), pp. 107-130.

Zienkiewicz, O.C.; Chan, A.H.C.; Pastor, M.; Paul, D.K.; Shiomi, T.(1990a):

Static and dynamic behaviour of soils: a rational approach to quantitative solutions. I - Fully saturated problems, *Proc. Roy. Soc. London*, A429, 285-309, 1990

Zienkiewicz, O.C.; Xie, Y.M.; Schrefler, B.A.; Ladesma, A.; Bicanic, N. (1990b): Static and dynamic behaviour of soils: a rational approach to quantitative solutions, part II: semi-saturated problems, *Proc. Roy. Soc. London,* A429,310-323

Zienkiewicz, O.C.; Chan, A.; Pastor, M.; Schrefler, B.A.; Shiomi, T. (1999): *Computational Geomechanics with special Reference to Earthquake Engineering*. John Wiley & Sons, Chichester.

Appendix

$$\mathbf{C}_{gg} = \int_B \mathbf{N}_p^T \left[(1-S_w)\, n \frac{M_a}{RT} + \frac{nS_w}{K_{ca}} \frac{\partial p^{ga}}{\partial p^g} \right] \mathbf{N}_p \, dV$$

$$\mathbf{C}_{gc} = \int_B \mathbf{N}_p^T \left[n\rho^{ga} \frac{\partial S_w}{\partial p^c} + S_g n \frac{M_w}{RT} \frac{\partial p^{gw}}{\partial p^c} + \frac{nS_w}{K_{ca}} \frac{\partial p^{ga}}{\partial p^c} \right] \mathbf{N}_p dV$$

$$\begin{aligned} \mathbf{C}_{gt} = & \int_B \mathbf{N}_p^T \left[n\rho^{ga} \frac{\partial S_w}{\partial T} - \rho^{ga} \beta_s (1-n)(1-S_w) \right] \mathbf{N}_t dV \\ & - \int_B \mathbf{N}_p^T \left[\frac{p^{ga}}{K_{ca}} \beta_s (1-n) S_w + \frac{nS_w}{K_{ca}} \frac{\partial p^{ga}}{\partial T} \right] \mathbf{N}_t dV \\ & + \int_B \mathbf{N}_p^T (1-S_w)\, n \left[-\frac{M_w}{RT} \left(\frac{\partial p^{gw}}{\partial T} - \frac{p^{gw}}{T} \right) - \frac{M_a}{T^2 R} \right] \mathbf{N}_t \, dV \end{aligned}$$

$$\mathbf{C}_{gu} = \int_B \mathbf{N}_p^T \left[\frac{p^{ga}}{K_{ca}} S_w + (1-S_w) \rho^{ga} \right] \mathbf{m}^T \mathbf{B} dV$$

$$\begin{aligned} \mathbf{K}_{gg} = & -\int_B (\nabla \mathbf{N}_p)^T \left[-\rho^{ga} \frac{\mathbf{k} k^{rg}}{\mu^g} - \frac{p^{ga}}{K_{ca}} \frac{\mathbf{k} k^{rw}}{\mu^w} \right] \nabla \mathbf{N}_p dV \\ & - \int_B (\nabla \mathbf{N}_p)^T \left[\rho^g \frac{M_a M_w}{M_g^2} \mathbf{D}_g^{ga} \left(-\frac{p^{gw}}{(p^g)^2} \right) \right] \nabla \mathbf{N}_p dV \end{aligned}$$

$$\mathbf{K}_{gc} = -\int_B (\nabla \mathbf{N}_p)^T \frac{p^{ga}}{K_{ca}} \frac{\mathbf{k} k^{rw}}{\mu^w} \nabla \mathbf{N}_p dV - \int_B (\nabla \mathbf{N_p})^T \left[\rho^g \frac{M_a M_w}{M_g^2} \mathbf{D}_g^{gw} \frac{1}{p^g} \frac{\partial p^{gw}}{\partial p^c} \right] \nabla \mathbf{N}_p dV$$

$$\mathbf{K}_{gt} = -\int_B (\nabla \mathbf{N_p})^T \left[\rho^g \frac{M_a M_w}{M_g^2} \mathbf{D}_g^{gw} \frac{1}{p^g} \frac{\partial p^{gw}}{\partial T} \right] \nabla \mathbf{N}_t dV$$

$$\mathbf{F}_g = -\int_B (\nabla \mathbf{N}_p)^T \left[\rho^{ga}\frac{\mathbf{k}k^{rg}}{\mu^g} + \frac{p^{ga}}{K_{ca}}\frac{\mathbf{k}k^{rw}}{\mu^w}\right]\rho^g \mathbf{g}\, dV + \int_{\partial B_g^q} \mathbf{N}_p^T q^{ga} dA + \int_{\partial B_C^q} \mathbf{N}_p^T \frac{\hat{p}^{ga}}{K_{ca}}\frac{q^w}{\rho^w} dA$$

$$\mathbf{C}_{cc} = \int_B \mathbf{N}_p^T \left[(1-S_w)\, n \frac{M_w}{RT}\frac{\partial p^{gw}}{\partial p^c} + n\left(\rho^w - \rho^{gw}\right)\frac{\partial S_w}{\partial p^c}\right]\mathbf{N}_p dV$$

$$\mathbf{C}_{ct} = \int_B \mathbf{N}_p^T \left[-S_w \beta_{swg} + (1-S_w)\, n \frac{M_w}{RT}\left(\frac{\partial p^{gw}}{\partial T} - \frac{p^{gw}}{T}\right)\right]\mathbf{N}_t dV + \int_B \mathbf{N}_p^T \left[n\left(\rho^w - \rho^{gw}\right)\frac{\partial S_w}{\partial T}\right]\mathbf{N}_t dV$$

$$\mathbf{C}_{cu} = \int_B \mathbf{N}_p^T \left[\rho^{gw}(1-S_w) + \rho^w S_w\right]\mathbf{m}^T \mathbf{B}\, dV$$

$$\mathbf{K}_{cg} = -\int_B (\nabla \mathbf{N}_p)^T \left[-\rho^{ga}\frac{M_a M_w}{M_g^2}\mathbf{D}_g^{gw}\left(-\frac{p^{gw}}{(p^g)^2}\right)\right]\nabla \mathbf{N}_p dV - \int_B (\nabla \mathbf{N}_p)^T \left[-\rho^{gw}\frac{\mathbf{k}k^{rg}}{\mu^g} - \rho^w \frac{\mathbf{k}k^{rw}}{\mu^w}\right]\nabla \mathbf{N}_p dV$$

$$\mathbf{K}_{cc} = \int_B (\nabla \mathbf{N}_p)^T \left[\rho^g \frac{M_a M_w}{M_g^2}\mathbf{D}_g^{gw}\left(\frac{1}{p^g}\frac{\partial p^{gw}}{\partial p^c}\right)\right]\nabla \mathbf{N}_p dV - \int_B (\nabla \mathbf{N}_p)^T \left[\rho^w \frac{\mathbf{k}k^{rw}}{\mu^w}\right]\nabla \mathbf{N}_p dV$$

$$\mathbf{K}_{ct} = -\int_B (\nabla \mathbf{N}_p)^T \left[-\rho^g \frac{M_a M_w}{M_g^2}\mathbf{D}_g^{gw}\frac{1}{p^g}\frac{\partial p^{gw}}{\partial T}\right]\nabla \mathbf{N}_t dV$$

$$\mathbf{F}_c = \int_B (\nabla \mathbf{N}_p)^T \left[\rho^{gw}\frac{\mathbf{k}k^{rg}}{\mu^g}\left(\rho^g \mathbf{g}\right) + \rho^w \frac{\mathbf{k}k^{rw}}{\mu^w}\left(\rho^w \mathbf{g}\right)\right] dV - \int_{\partial B_c^q} \mathbf{N}_p^T \left[q^w + q^{gw} + \beta_c\left(\rho^{gw} - \rho_\infty^{gw}\right)\right] dA$$

$$\mathbf{C}_{tc} = \int_B \mathbf{N}_t^T \Delta H_{vap}\left[-\rho^w n \frac{\partial S_w}{\partial p^c}\right]\mathbf{N}_c dV$$

$$\mathbf{C}_{tt} = \int_B \mathbf{N}_t^{\mathbf{T}}\left[\left(\rho C_p\right)_{eff} + \beta_{sw}\rho^w - \rho^w n \frac{\partial S_w}{\partial T}\right]\mathbf{N}_t\, dV$$

$$\mathbf{C}_{tu} = \int_B \mathbf{N}_t^T \Delta H_{vap} \left(-\rho^w S_w\right) \mathbf{m}^T \mathbf{B}\, dV$$

$$\mathbf{K}_{tg} = \int_B \mathbf{N}_t^T \left[-\rho^w C_p^w \frac{\mathbf{k} k^{rw}}{\mu^w}\right] \left(\nabla \mathbf{N}_p \cdot \nabla T\right) dV + \int_B \mathbf{N}_t^T \left[-\rho^g C_p^g \frac{\mathbf{k} k^{rg}}{\mu^g}\right] \left(\nabla \mathbf{N}_p \cdot \nabla T\right) dV$$
$$+ \int_B \left(\nabla \mathbf{N}_t\right)^T \Delta H_{vap} \left[-\rho^w \frac{\mathbf{k} k^{rw}}{\mu^w}\right] \nabla \mathbf{N}_p dV$$

$$\mathbf{K}_{tc} = \int_B \mathbf{N}_t^T \left[\rho^w C_p^w \frac{\mathbf{k} k^{rw}}{\mu^w}\right] \left(\nabla \mathbf{N}_p \cdot \nabla T\right) dV + \int_B \left(\nabla \mathbf{N}_t\right)^T \Delta H_{vap} \left[\rho^w \frac{\mathbf{k} k^{rw}}{\mu^w}\right] \nabla \mathbf{N}_p dV$$

$$\mathbf{K}_{tt} = \int_B \left(\nabla \mathbf{N}_t\right)^T \chi_{eff} \nabla \mathbf{N}_t\, dV + \int_B \mathbf{N}_t^T \left[\rho^w C_p^w \frac{\mathbf{k} k^{rw}}{\mu^w} \left(-\nabla p^g + \nabla p^c + \rho^w \mathbf{g}\right)\right] \cdot \nabla \mathbf{N}_t\, dV$$
$$+ \int_B \mathbf{N}_t^T \left[\rho^g C_p^g \frac{\mathbf{k} k^{rg}}{\mu^g} \left(-\nabla p^g + \rho^g \mathbf{g}\right)\right] \cdot \nabla \mathbf{N}_t\, dV$$

$$\mathbf{F}_t = -\int_B \mathbf{N}_t^T \left[\rho^w C_p^w \frac{\mathbf{k} k^{rw}}{\mu^w} \left(\rho^w \mathbf{g}\right)\right] \cdot \nabla T\, dV - \int_B \mathbf{N}_t^T \left[\rho^g C_p^g \frac{\mathbf{k} k^{rg}}{\mu^g} \left(\rho^g \mathbf{g}\right)\right] \cdot \nabla T\, dV$$
$$- \int_B \left(\nabla \mathbf{N}_t\right)^T \Delta H_{vap} \left[\rho^w \frac{\mathbf{k} k^{rw}}{\mu^w} \left(\rho^w \mathbf{g}\right)\right] dV$$
$$- \int_{\partial B_T^q} \mathbf{N}_t^T \left[q^T + \alpha_c \left(T - T_\infty\right) + e\, \sigma_o \left(T^4 - T_\infty^4\right)\right] dA$$

$$\mathbf{K}_{ug} = -\int_B \mathbf{B}^T \mathbf{m}^T \mathbf{N}_p\, dV$$

$$\mathbf{K}_{uc} = \int_B \mathbf{B}^T \mathbf{m}^T S_w \mathbf{N}_p\, dV$$

$$\mathbf{K}_{ut} = -\int_B \mathbf{B}^T \mathbf{D}^e \frac{\beta_s}{3} \mathbf{m}^T \mathbf{N}_t\, dV$$

$$\mathbf{K}_{uu} = \int_B \mathbf{B}^T \sigma'_{\mathrm{m}}\, dV$$

$$\mathbf{F}_u = \int_B -\mathbf{B}^T \mathbf{D}^e \left[\frac{\beta_s}{3} T_0\right] \mathbf{m}^T dV - \int_{\partial B_u^q} \mathbf{N}_u^T \mathbf{t}\, dA$$
$$- \int_B \mathbf{N}_u^T \left[(1-n)\rho^s + nS_w\rho^w + n(1-S_w)\rho^g\right] \mathbf{g}\, dV$$

With:

B = L $\mathbf{N}_u$ strain operator matrix

L = differential operator matrix of the kinematic equations

$\mathbf{D}^e$ = elastic stiffness matrix

σ'_m = mechanical effective stress tensor

∇ = gradient operator

CMES: Computer Modeling in Engineering & Sciences

ISSN : 1526-1492 (Print); 1526-1506 (Online)

Journal website:
http://www.techscience.com/cmes/

Manuscript submission
http://submission.techscience.com

Published by
Tech Science Press
5805 State Bridge Rd, Suite G108
Duluth, GA 30097-8220, USA

Phone (+1) 678-392-3292
Fax (+1) 678-922-2259
Email: sale@techscience.com
Website: http://www.techscience.com
Subscription: http://order.techscience.com

CMES is Indexed & Abstracted in
Applied Mechanics Reviews; Cambridge Scientific Abstracts (Aerospace and High Technology; Materials Sciences & Engineering; and Computer & Information Systems Abstracts Database); CompuMath Citation Index; Current Contents: Engineering, Computing & Technology; Engineering Index (Compendex); INSPEC Databases; Mathematical Reviews; MathSci Net; Mechanics; Science Alert; Science Citation Index; Science Navigator; Zentralblatt fur Mathematik.